Exhumation and uplift of the Sierras Pampeanas: preliminary implications from K–Ar fault gouge dating and low-T thermochronology in the Sierra de Comechingones (Argentina)

Stefan Löbens · Frithjof A. Bense · Klaus Wemmer ·
István Dunkl · Carlos H. Costa · Paul Layer ·
Siegfried Siegesmund

Abstract The Sierras Pampeanas in central and north-western Argentina constitute a distinct morphotectonic feature between 27°S and 33°S. The last stage of uplift and deformation in this area are interpreted to be closely related to the Andean flat-slab subduction of the Nazca plate beneath the South American plate. K–Ar fault gouge dating and low-temperature thermochronology along two transects within the Sierra de Comechingones reveal a minimum age for the onset of brittle deformation about 340 Ma, very low exhumation rates since Late Paleozoic time, as well as a total exhumation of about 2.3 km since the Late Cretaceous. New Ar–Ar ages (7.54–1.91 Ma) of volcanic rocks from the San Luis volcanic belt support the eastward propagation of the flat-slab magmatic front, confirming the onset of flat-slab related deformation in this region at 11.2 Ma. Although low-temperature thermochronology does not clearly constrain the signal of the Andean uplift, it is understood that the current structural relief related to the Comechingones range has been achieved after the exhumation of both fault walls (circa 80–70 Ma).

Keywords Sierras Pampeanas · K–Ar dating · Fault gouge dating · Low thermal geochronology · Andean uplift

S. Löbens (✉) · F. A. Bense · K. Wemmer · I. Dunkl ·
S. Siegesmund
Geoscience Centre, University of Göttingen,
Goldschmidtstr. 3, 37077 Göttingen, Germany
e-mail: stefan.loebens@geo.uni-goettingen.de

C. H. Costa
Departamento de Geología, Universidad Nacional de San Luis,
Chacabuco 917, 5700 San Luis, Argentina

P. Layer
Department of Geology and Geophysics, University of Alaska,
900 Yukon Drive, Fairbanks, AK 99775, USA

Introduction

The Sierras Pampeanas in central and north-western Argentina represent an area of N–S trending mountain ranges showing elevations of up to 5,550 m that are divided by intermountain basins (Fig. 1; González Bonorino 1950; Caminos 1979; Jordan and Allmendinger 1986; Ramos et al. 2002; among others). Mainly consisting of Late Pre-Cambrian to Early Paleozoic basement rocks, i.e. igneous and metamorphic rocks (e.g. González Bonorino 1950; Caminos 1979; Gordillo and Lencinas 1979), these mountain ranges comprise twelve main tectonic blocks (Jordan and Allmendinger 1986), which represent distinct morphotectonic features above the shallowing Nazca plate within the area of 27°S–33°S east of the Precordillera (e.g. Jordan et al. 1983; Jordan and Allmendinger 1986; Ramos et al. 2002 and many others). The uplift and type of deformation of the Sierras Pampeanas is interpreted to be closely related to the flat-slab subduction of the Nazca plate beneath the South American plate since the Miocene and after the collision of the Juan Fernández Ridge (e.g. Jordan et al. 1983; Yañez et al. 2001; Ramos et al. 2002).

Two main morphotectonic features stand out at most of these faulted blocks: a topographic asymmetry, with a steep western slope and a gentle eastern slope where preserved remains of erosion surfaces stand out. Such paleolandsurfaces have traditionally been envisaged as a continuous and essentially synchronous surface, exhumed and disrupted during the Andean orogeny (González Díaz 1981; Criado Roque et al. 1981). However, Jordan et al. (1989) suggested that these erosion surfaces are diachronic in age at a regional scale. Later, Carignano et al. (1999) postulated that many paleosurfaces scarps and slope breaks result from juxtaposition of diachronous surfaces (ranging from

Late Paleozoic to Paleogene ages), rather than being a consequence of the Andean tectonism.

Current uncertainties about the ages and evolutionary paths of these currently exposed erosion surfaces preclude a suitable analysis of core issues regarding the tectonic evolution of the Sierras Pampeanas (i.e. the structural relief related to the Andean orogeny).

In order to investigate the Neogene uplift and exhumation (as defined by England and Molnar 1990) history of the Sierras Pampeanas, low temperature thermochronologic dating methods, e.g. apatite fission track and (U-Th)/He dating, can provide constraints, because these techniques are suitable to constrain time, amounts and rate of cooling/erosion associated with mountain building, crustal deformation, extensional tectonics and landscape evolution (e.g. Gallagher et al. 1998; Farley 2002; Ehlers et al. 2003; Stockli et al. 2000; Fitzgerald et al. 2006). To contribute to the knowledge of the exhumation history of the Sierras Pampeanas as well as an attempt to clarify its relationship to the Andean flat-slab subduction, we followed three different approaches investigating two different elevation profiles in the Sierra de Comechingones. We performed (a) K–Ar dating on illite fine fractions from brittle fault gouges to examine the brittle deformation history (b) apatite fission track analysis and (U-Th)/He measurements of zircon and apatite, to reconstruct the exhumation and uplift history of the Sierra de Comechingones and to extend the post-metamorphic cooling path of basement (Steenken et al. 2010) to the low-temperature thermal history, as well as (c) Ar–Ar dating on volcanic rocks to evaluate the youngest flat-slab subduction-related magmatism possibly indicating the eastward migration of the deformation into the foreland (e.g. Ramos et al. 2002).

Regional setting and geodynamic evolution

The basement complex of the Sierras Pampeanas was developed by accretion of different allochthonous and parautochthonous terranes during the Late Proterozoic and the Early Paleozoic (e.g. Ramos 1988, 2009; Ramos et al. 2002; Steenken et al. 2004; Miller and Söllner 2005). Potential sutures indicating the margins of adjacent terranes, e.g. Río del la Plata Craton, Pampia, and Cuyania, are illustrated by Ramos et al. (2001, 2002).

During the Late Triassic—Early Jurassic and the Early Cretaceous, the basement was affected by extensional deformation (e.g. Uliana et al. 1989; Ramos et al. 2002), whereby the latter period was related to the opening of the South Atlantic Ocean at these latitudes (Uliana et al. 1989; Rossello and Mozetic 1999). According to Ramos et al. (2002), master faults related to the rift events were

Fig. 1 Schematic overview of the Sierras Pampeanas with the main thrusts (modified after Ramos et al. 2002). The mountain ranges are shown in grey and intermountain basins are white but not named. For reference, a schematic map of Argentina is shown in the *upper left*, where the *grey frame* marks the area of the Sierras Pampeanas. The *red stars* indicate the sample locations (La Carolina volcanic field in the west and Sierra del Morro in the east) of volcanic rocks taken for Ar–Ar analysis

generated by reactivating the sutures between the different cratonic terranes. Continental basins, usually with a half-graben geometry, were developed all over this region, recording mostly the Early Cretaceous stages of rifting (Schmidt et al. 1995).

The extensional fault systems were inverted during the Andean compression caused by subduction of the Nazca Plate beneath the South American plate in the Cenozoic, thus controlling the inception and uplift of the basement blocks forming the Sierras Pampeanas. Accordingly, these basement uplifts have been recognised as a broken foreland of the Andean orogeny (Jordan and Allmendinger 1986) and regarded to be part of the Andean building (Regnier et al. 1992; Costa et al. 2006). The geometry of these reverse faults and thrusts is controlled by basement structures generally resulting in a listric shape and a dominant dip to the east, which is expressed by the referred morphologic asymmetry of the basement blocks (Fig. 2a, b; e.g. González Bonorino 1950; Gordillo and Lencinas 1979; Criado Roque et al. 1981; González Díaz 1981; Jordan and Allmendinger 1986; Introcaso et al. 1987; Massabie 1987; Costa and Vita Finzi 1996; Ramos et al. 2002).

Within Miocene times (18–11 Ma), the Juan Fernández ridge is incorporated into the subduction (Fig. 3; e.g. Yañez et al. 2001; Ramos et al. 2002) resulting in a shallowing of the Nazca Plate subduction angle (Barazangi and Isacks 1976; Pilger 1981; Jordan and Allmendinger 1986). This flat-slab subduction (Fig. 4) is set to be indicated by (a) the depth of the Wadati-Benioff zone (b) a gap of active arc volcanism between 27°S and 33°S (c) the uplift and deformation of Sierras Pampeanas starting at the Late Miocene-Pliocene transition, and (d) the timing and location of magmatic activity within the area of the Sierras Pampeanas broken foreland (e.g. Barazangi and Isacks 1976; Pardo Casas and Molnar 1987; Smalley and Isacks 1987, 1990; Cahill and Isacks 1992; Ramos et al. 2002; and references therein).

During the Upper Miocene and the Pliocene the outcropping area of magmatic and hydrothermal activity was shifted eastward to the eastern part of the Sierras Pampeanas (Kay et al. 1991). Here, volcanic buildings crop out along a WNW trending belt between the volcanic field of La Carolina (Fig. 5) in the west and the Sierra del Morro in the east, standing out from the erosion surfaces smooth
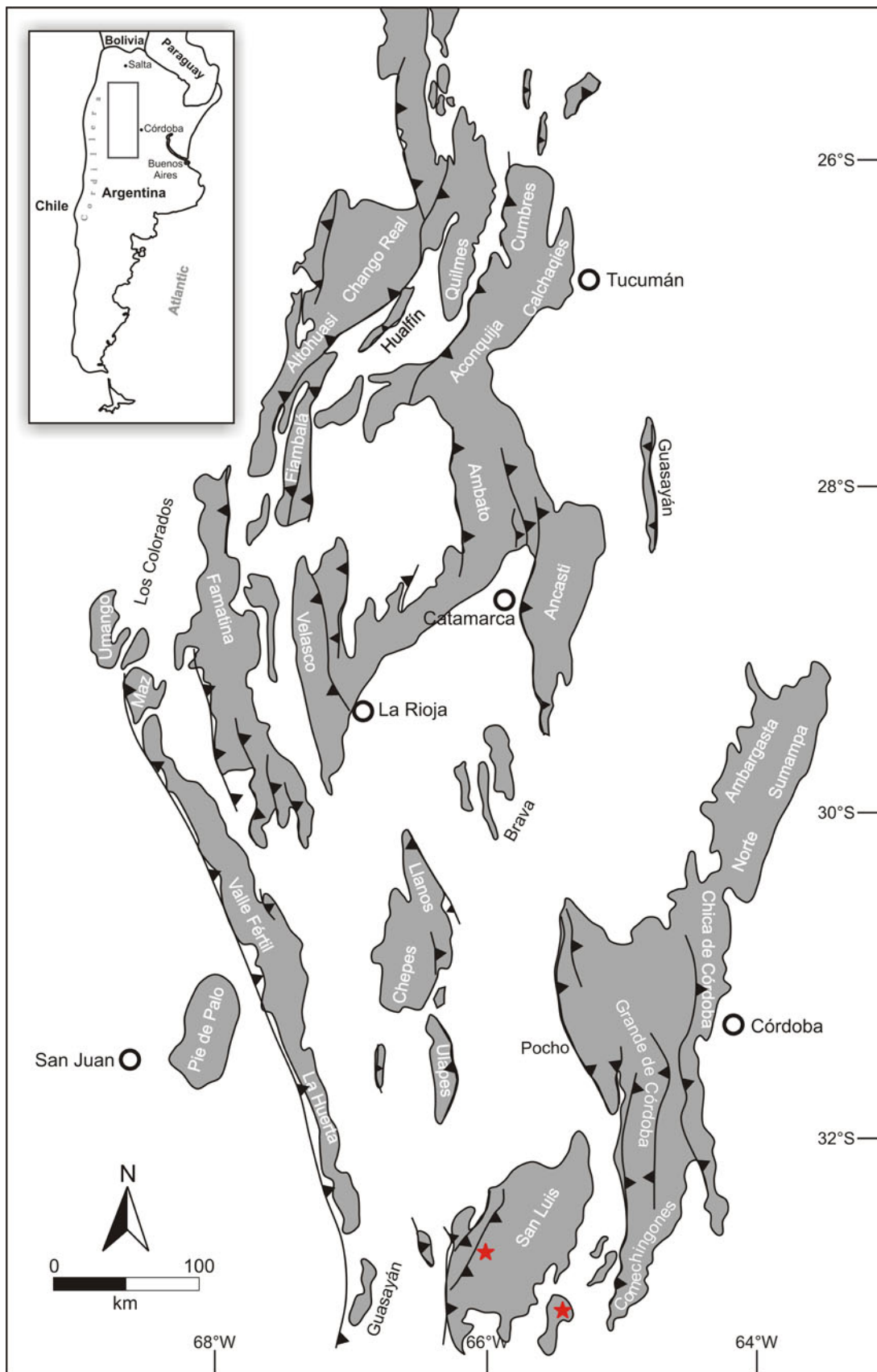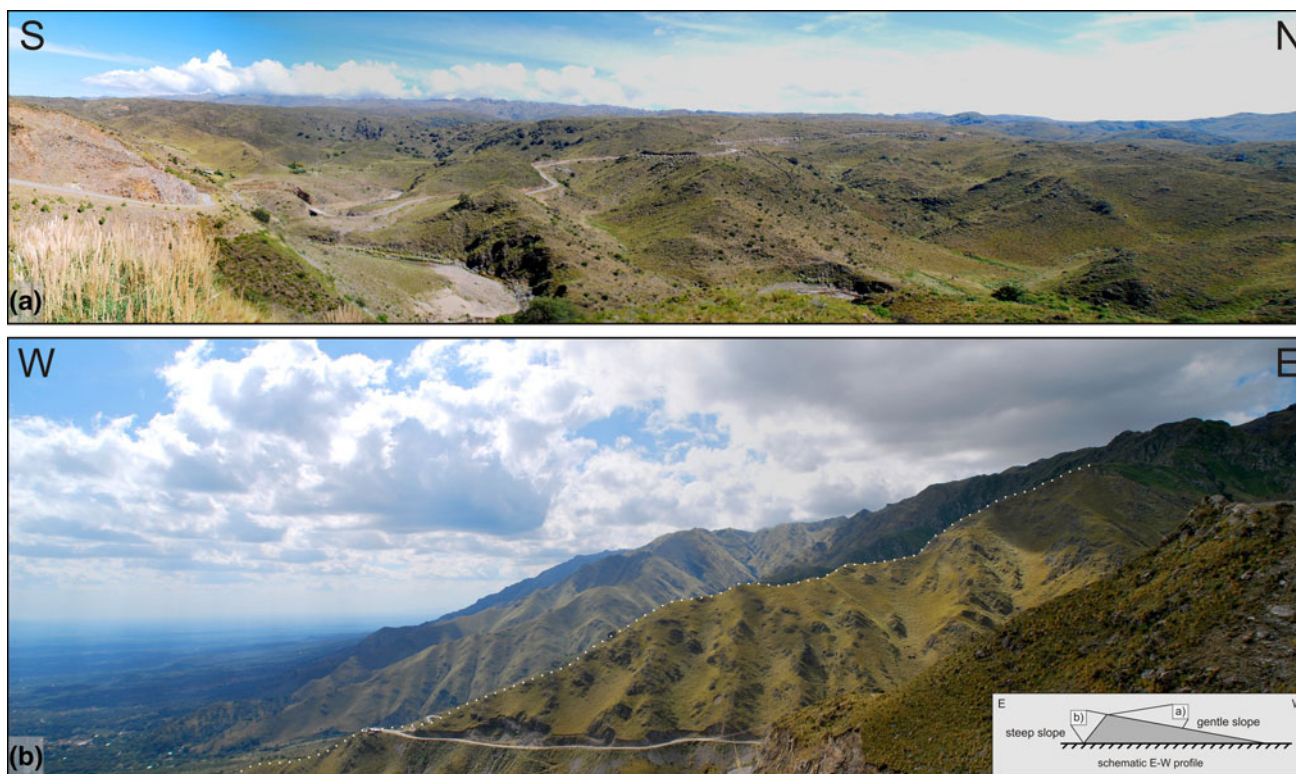
Fig. 2 Photographs showing the two extremities of relief within the Sierras Pampeanas. **a** The gentle inclined, low relief slope on the eastern side of the Sierras de San Luis near the village of El Trapiche (view to the west). **b** The steep inclined, high relief slope on the western side of the Sierra de Comechingones near the village of Merlo (view to the *north*). The schematic sketch in the *lower right* indicates point of view
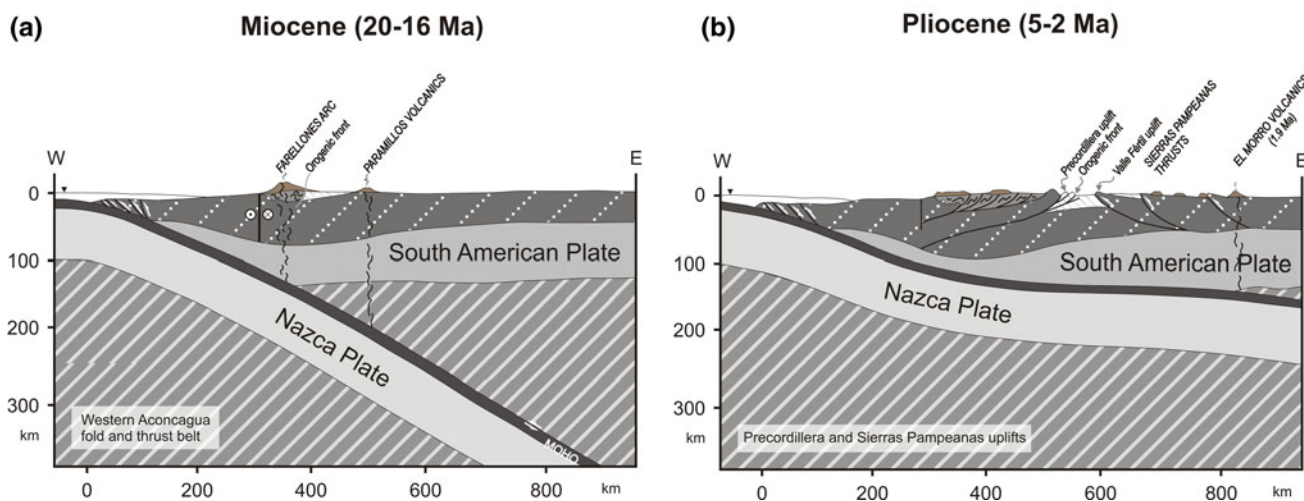

Fig. 3 Evolutional stages of the Andean system, including the Sierras Pampeanas, related to the shallowing Nazca plate during the Cenozoic (modified after Ramos et al. 2002). **a** Subduction prior to the collision of the Juan Fernandez Ridge. **b** Last stage of arc-related magmatism within the Sierra del Morro prior to the present setting

landscape. Theses rocks comprise andesites, dacites, latites, trachytes and hydrothermal altered rocks showing decreasing ages from 11.2 to 6.3 Ma in the west to 1.9 Ma in the east (Llambías and Brogiono 1981; Sruoga et al. 1996; Urbina et al. 1997; Urbina 2005; Ramos et al. 1991, 2002;

Urbina and Sruoga 2008, 2009; and this study). Further, these volcanic rocks show a typical subduction signature (Kay et al. 1991; Kay and Gordillo 1994), thus marking the easternmost and youngest magmatic manifestation associated with the shallowing of the Nazca plate in the Andean

Fig. 4 Schematic sketch of the shallowing Nazca Plate (modified from Kerrich et al. 2000; Urbina 2005). The ages for Cerro Tomolasta and El Morro are from this publication. The ages for the Farallón Negro Volcanic District represent K–Ar data from Ramos et al. (1991)
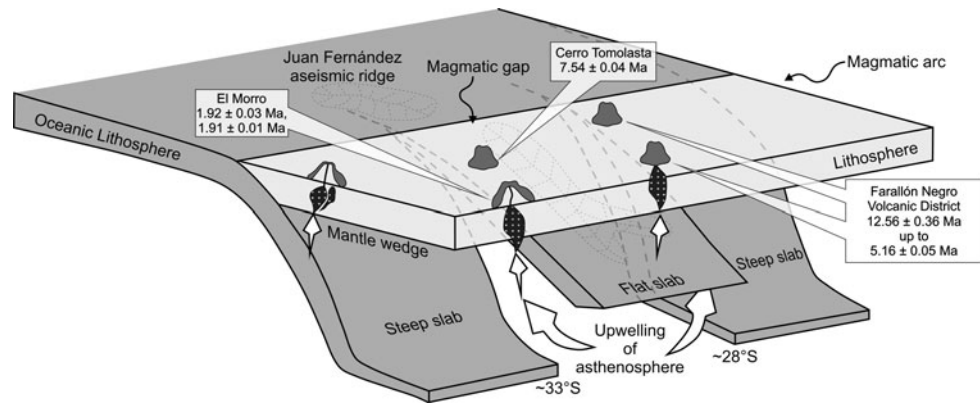
Fig. 5 Photograph showing the Late Miocene volcanic body of the Cerro Tomolasta in the La Carolina area (view from the Pampa de la Invernada towards the east). The volcanic edifices build up hills, dominating the landscape on the otherwise flat eastern hillslope of the Sierra de San Luis

flat-slab segment located 650–750 km east of the Peru–Chile trench (e.g. Ramos et al. 1991; 2002).

The uplift of the south-eastern Sierras Pampeanas, e.g. Sierra de San Luis, Comechingones, and El Morro, as well as the termination of the magmatism within the Sierra del Morro in the Late Pleistocene have been interpreted as the last stage of the Andean uplift (Costa 1992; Ramos et al. 2002). Subduction-related shortening and deformation in the Sierras Pampeanas during the Quaternary is mainly accommodated by the ranges bounding reverse faults mostly located at the western footslope of the sierras (Massabie 1976, 1987; Costa 1987, 1992, 1996, 1999; Kramer et al. 1995; Costa and Vita Finzi 1996; Costa et al. 2001; 2006).

Applied methods

Mineralogy and K–Ar dating of fault gouges

In brittle near-surface faults, rocks are broken and crushed by tectonic movements. In these localised zones, the increased surface creates a high chemical reactivity, allowing retrograde processes to produce fault gouges composed of authigenic hydrosilicates such as illite. Thus, formation time of the authigenic illite in a fault gouge can be correlated with periods of motion along the fault (e.g. Lyons and Snellenburg 1971; Kralik et al. 1987).

The illite crystallinity (IC) and polytypism are important indices for determining the grade of thermal evolution and very low-grade metamorphism grades. The IC values, which are inversely proportional to the illite crystallinity, are defined after Kübler (1964) as half-height width of the 10 Å XRD peak. The values for the illite crystallinity may range from 0.06 $\Delta°2\theta$ for ideally ordered muscovite up to 1 $\Delta°2\theta$ for illite/smectite mixed layers (Kübler 1964, 1967, 1968).

Kübler (1967) used boundary values of 0.42 $\Delta°2\theta$ and 0.25 $\Delta°2\theta$ to divide the zones of the very low-grade metamorphism into, from lower to higher grade, diagenetic zone (IC > 0.42 $\Delta°2\theta$), anchizone (0.42 $\Delta°2\theta$ < IC > 0.25 $\Delta°2\theta$) and epizone (IC < 0.25 $\Delta°2\theta$), in which the corresponding temperatures for the two boundaries are around 150°C and 300°C, respectively.

Thus, the IC values of authigenic fault gouge illite can be used to estimate the temperature experienced by the fault gouge sample. This information helps to interpret the dating results concerning the thermal evolution.

Polytypism (Bailey et al. 1977; Guinier et al. 1984) is a common phenomenon for layered silicate minerals such as mica, chlorite and kaolinite. For illite, the most common polytypes are the $1 M_d$, $1M$ and $2M_1$ (e.g. Reynolds and Thomson 1993). With raising temperature, illite shows irreversible polytype transformation of $1 M_d \rightarrow 1M \rightarrow 2M_1$ (Hunziker et al. 1986). Generally, illite has $1 M_d$ and $1 M$ polytypes in a diagenetic zone, a mixture of 1M and $2M_1$ polytypes in the anchizone and sole $2M_1$ polytypes in the epizone (e.g. Bailey 1966; Środoń and Eberl 1984).

We measured a total of six fault gouge samples taken from the Merlo profile (Fig. 6). Details on the analytical procedure are given in the appendix.

Apatite fission track and (U-Th)/He thermochronology

The combination of apatite fission track dating (AFT) as well as (U-Th)/He dating on zircon (ZHe) and apatite (AHe) allows the reconstruction of low-temperature exhumation history (e.g. Hurley 1954; Armstrong 1966; Wagner and van Den Haute 1992; Farley et al. 1996; Wolf et al. 1996). The thermal sensitivity of the apatite fission track method referred to as partial annealing zone (PAZ; Gleadow and Fitzgerald 1987) ranges between 130 and
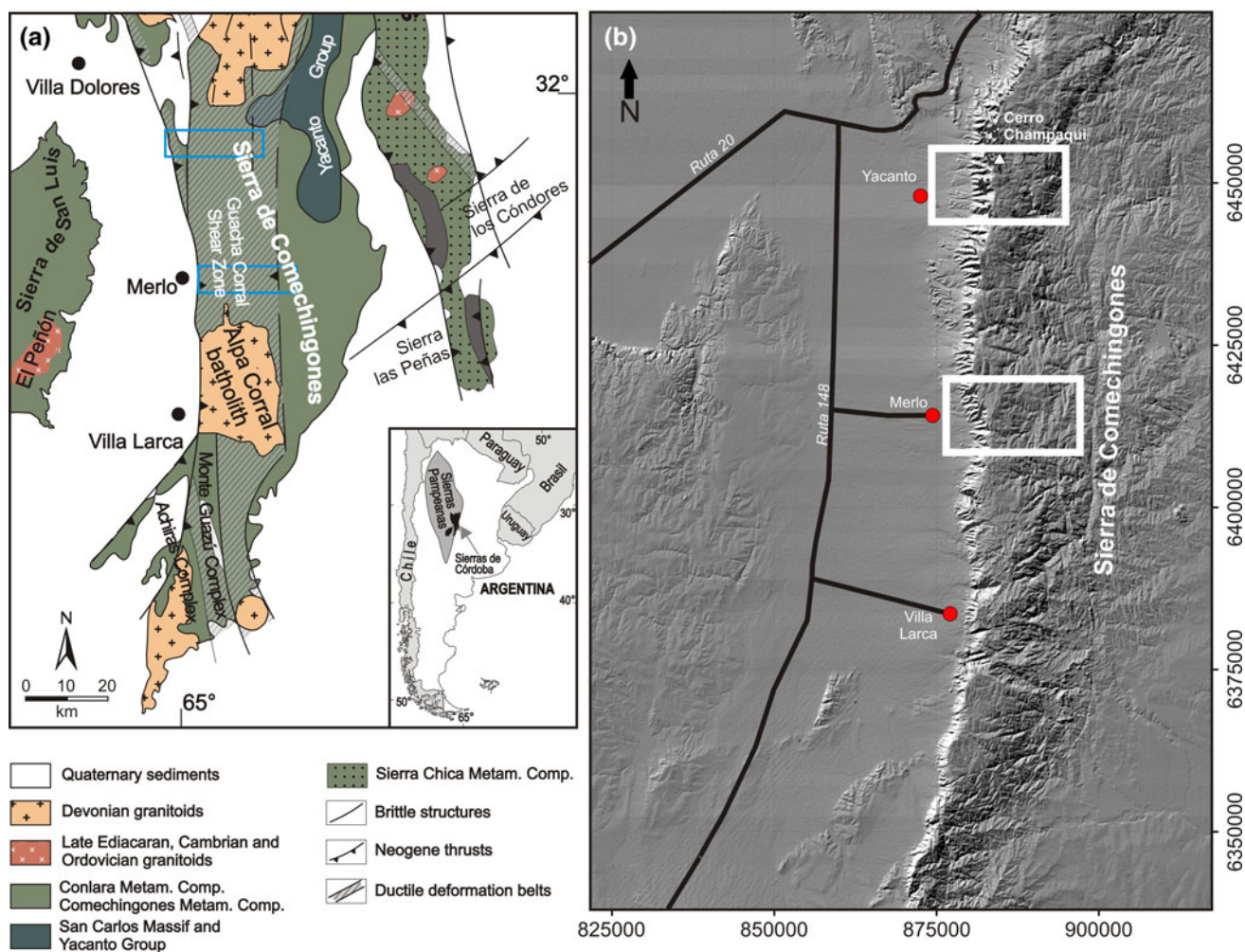
Fig. 6 Overview of the working area. **a** Schematic geological map of the Sierra de Comechingones (modified after Steenken et al. 2010). The coordinates are given in longitude and latitude. The blue frames mark both sampled profiles (referred to as Merlo and Yacanto profile in the text). For reference, a schematic map of Argentina, including the Sierras Pampeanas, is shown in the *lower right*. **b** Digital elevation model of the working area. The coordinates are given in UTM coordinates. The white frames define the sampled profiles

70°C (e.g. Donelick et al. 1999; Ketcham et al. 1999). Regarding the (U-Th)/He method this interval is called partial retention zone (PRZ; e.g. Baldwin and Lister 1998; Wolf et al. 1998). The temperature of the PRZ for the (U-Th)/He system ranges from around 65°C to approximately 30°C for apatite and from about 185°C to 135°C for zircon (e.g. Reiners and Brandon 2006).

A total of eight samples were collected from the Yacanto profile (Fig. 6). Three of them were dated by the AFT and ZHe method. AHe ages were obtained from all samples. Details on the analytical procedure are given in the appendix.

Ar–Ar dating of volcanic rocks

Ar–Ar ages in volcanic rocks can be interpreted as the age of effusion as closing temperatures for different mineral species are negligible due to rapid cooling (e.g. McDougall and Harrison 1999). In this study, Ar–Ar dating was performed following standard methods quoted elsewhere (e.g. Layer et al. 1987).

Hornblende and whole rock samples of three trachyandesites from discrete exposures have been dated (Fig. 1).

Details on the analytical procedure are given in the appendix.

Results

K–Ar dating

Eighteen K–Ar ages from fractions of six samples were obtained from the Merlo profile (Fig. 6) in this study (Table 1; Fig. 7). The ages range from Early Mississippian to Early/Middle Jurassic (342–174 Ma).

All samples show an age gap between fractions, ranging from 1.5 Ma up to 53.3 Ma (Fig. 8). Only the two smallest fractions of sample APG 82-09 show overlapping ages within error.

Radiogenic ^{40}Ar content ranges from 81.0 to 99.7% indicating reliable analytical conditions for all analyses. Potassium contents range from 1.03% (APG 82-09, <0.2 μm) to 5.88% (APG 85-09, 2–6 μm).

XRD analyses of all samples confirm that illite, chlorite and kaolinite are the major clay mineral components in the various fractions, with minor traces of

Table 1 K–Ar ages, illite crystallinity and illite polytypism of the investigated mineral fractions

Sample no.	Grain-size fraction	K–Ar data					Illite crystallinity		Illite polytypism
		K_2O [wt%]	$^{40}Ar^a$ [nl/g] STP	$^{40}Ar^a$ [%]	Age [Ma]	±2σ-error [Ma]	Air dry [$\Delta°2\theta$]	Glycolated [$\Delta°2\theta$]	
APG 82-09	<0.2 μm	1.03	8.68	89.80	244.0	6.1	0.281[c]	0.244[d]	1Md > 2M$_1$ > 1 M
	<2 μm	1.69	14.04	84.69	240.9	6.3	0.282[c]	0.275[c]	1Md > 2M$_1$ > 1 M
	2–6 μm	4.90	43.71	91.79	257.3	5.6	0.180[d]	0.211[d]	2M$_1$ ≥ 1Md > 1M
APG 85-09	<0.2 μm	2.33	18.84	89.63	234.8	5.0	0.491[b]	0.373[c]	1Md > 2M$_1$ > 1 M
	<2 μm	3.32	30.62	95.52	265.5	5.7	0.296[c]	0.272[c]	1Md > 2M$_1$ > 1 M
	2–6 μm	5.88	57.14	94.81	278.6	5.9	0.161[d]	0.164[d]	2M$_1$ > 1Md > 1M
APG 89-09	<0.2 μm	1.44	8.68	87.39	177.9	4.5	0.428[b]	0.377[c]	1Md > 2M$_1$ > 1 M
	<2 μm	2.58	19.73	96.69	222.7	7.0	0.273[c]	0.234[d]	1Md > 2M$_1$ > 1 M
	2–6 μm	5.37	48.27	98.17	259.2	5.5	0.163[d]	0.155[d]	2M$_1$ > 1Md > 1M
APG 90-09	<0.2 μm	1.62	9.54	81.01	174.0	4.9	0.530[b]	0.332[c]	1Md > 2M$_1$ > 1 M
	<2 μm	2.33	17.41	91.56	218.0	6.1	0.400[c]	0.313[c]	1Md > 2M$_1$ > 1 M
	2–6 μm	3.61	33.65	97.03	268.1	5.7	0.171[d]	0.173[d]	2M$_1$ > 1Md > 1M
APG 91-09	<0.2 μm	2.11	17.05	93.43	234.6	6.7	0.390[c]	0.358[c]	1Md > 2M$_1$ > 1 M
	<2 μm	3.39	35.67	97.11	299.9	6.4	0.272[c]	0.266[c]	2M$_1$ > 1Md > 1M
	2–6 μm	4.17	48.81	98.55	330.7	7.1	0.187[d]	0.179[d]	2M$_1$ ≫ 1Md > 1M
APG 92-09	<0.2 μm	2.21	18.62	95.07	244.0	5.7	0.441[b]	0.331[c]	1Md > 2M$_1$ > 1 M
	<2 μm	3.57	38.97	98.65	310.2	7.2	0.260[c]	0.247[d]	2M$_1$ > 1Md > 1M
	2–6 μm	3.81	46.21	98.44	341.6	7.9	0.168[d]	0.170[d]	2M$_1$ ≫ 1Md > 1M

STP standard pressure and temperature conditions, > more, ≫ much more

[a] Radiogenic, [b] diagenetic, [c] anchizonal, [d] epizonal
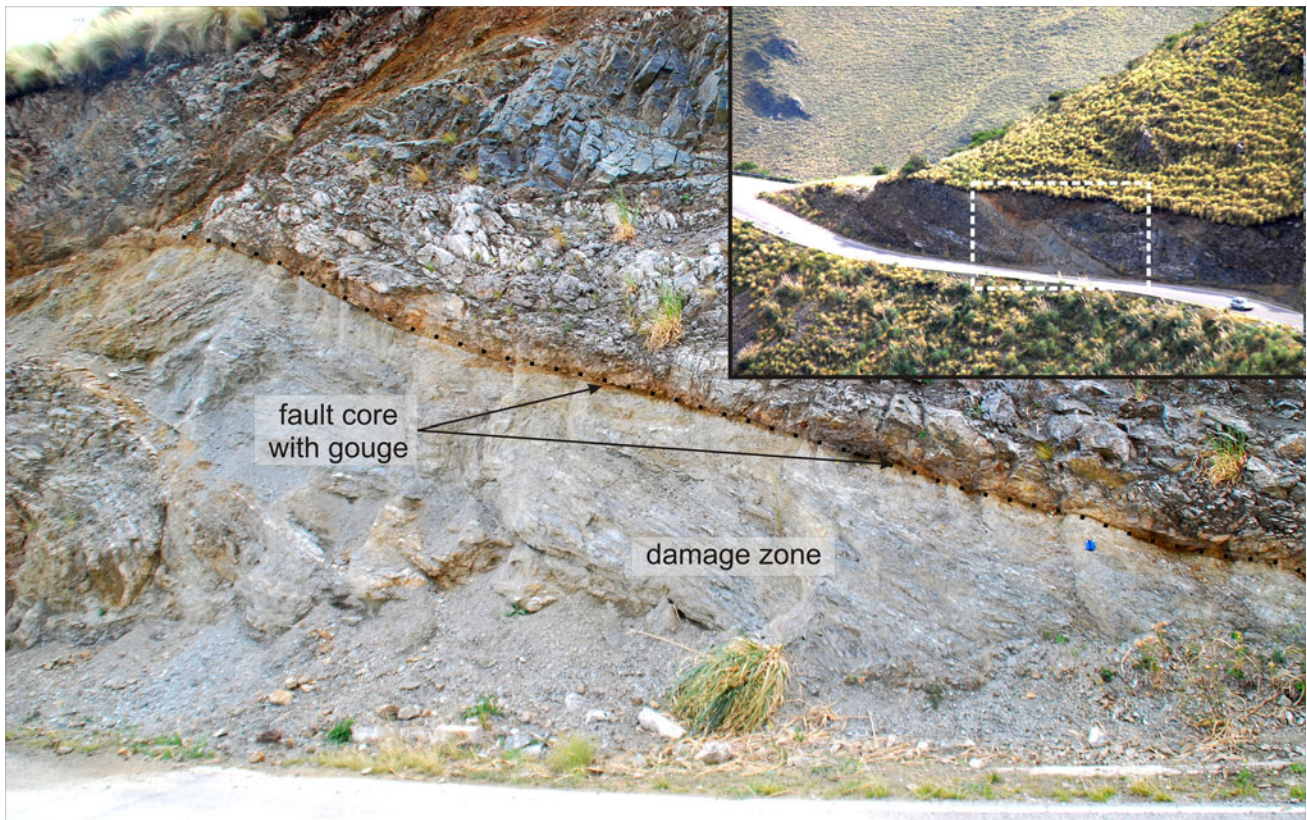
Fig. 7 Pictures of a brittle fault zone with a broad cataclastic zone and an approximately 8 cm wide fault gouge (sample APG 90-09) on the western slope of the Sierra de Comechingones, east of the village of Merlo (car in top right picture for scale, in lower picture blue compass on right side for scale)

Fig. 8 K–Ar ages with error bars (2σ) of all analysed grain-size fractions and samples
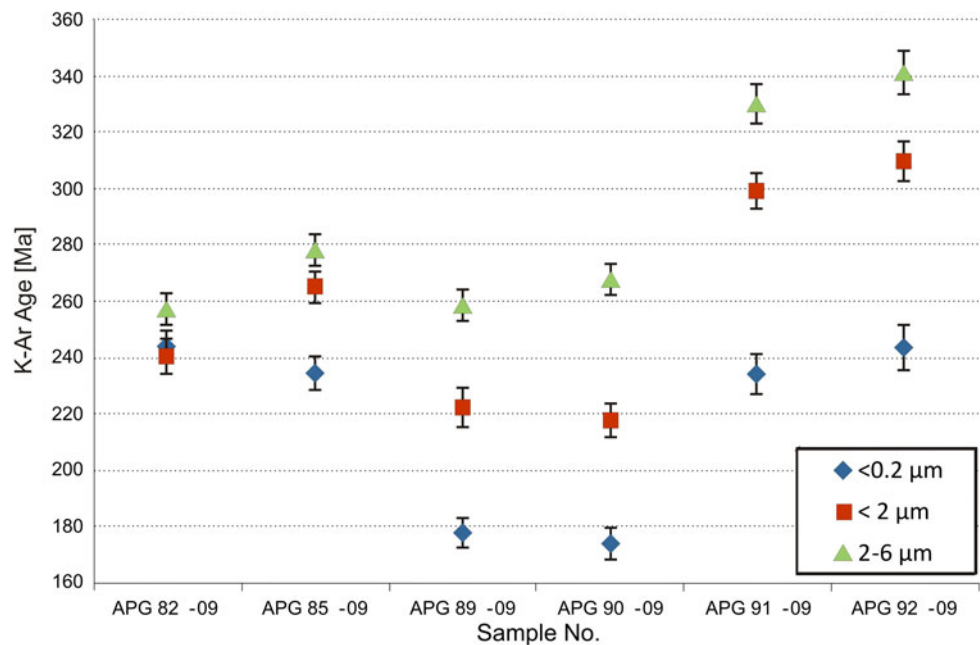
quartz in almost all sample fractions. Minor traces of potassium-feldspar might be present in the 2–6 μm fractions but none is found in the <0.2 μm and <2 μm fractions. Glycolated XRD analyses were carried out to investigate the potential occurrence of expandable mixed layers of illite and smectite. Major amounts of illite/smectite were found in the <0.2 μm fraction and minor amounts also in the <2 μm fractions. No illite/smectite

Table 2 Results of X-ray diffraction analyses from the sample material fractions

Sample no.	Grain-size fraction	Mineralogy					
		Illite	Chlorite	Kaolinite	Smectite	Quartz	K-feldspar
APG 82-09	<0.2 μm	+	+	o/−	−	o	−
	<2 μm	+	+	o/−	+	−	−
	2–6 μm	+	+	o/−	o	−	−
APG 85-09	<0.2 μm	+	−	+	+	o	−
	<2 μm	+	o	+	o	o	−
	2–6 μm	+	−	o	−	+	o/−
APG 89-09	<0.2 μm	o	+	o	++	−	−
	<2 μm	+	+	+	o	o	−
	2–6 μm	+	+	+	−	o	o/−
APG 90-09	<0.2 μm	+	−	+	+	−	−
	<2 μm	+	o	+	o	o	−
	2–6 μm	o	o	+	−	+	o/−
APG 91-09	<0.2 μm	+	+	−	+	−	−
	<2 μm	+	+	+	o	o	−
	2–6 μm	+	+	+	−	+	o/−
APG 92-09	<0.2 μm	o	+	o	+	−	−
	<2 μm	+	+	o/−	o	−	−
	2–6 μm	+	++	o	−	+	o/−

++ = dominant, + = abundant, o = less abundant, o/− = unclear, possibly traces, − none

mixed layers were observed in the 2–6 μm fractions (Table 2).

The illite crystallinity (IC) of all analysed samples varies from 0.155 $\Delta°2\theta$ to 0.530 $\Delta°2\theta$ (Table 1). The IC values from the air-dried <0.2 μm fractions indicate that all but one developed under diagenetic conditions, whereas the fractions of <2 μm and 2–6 μm yield anchi- to epimetamorphic values. Variations in the $\Delta°2\theta$ between the glycolated and the air-dry measurements correspond to the presence of illite/smectite mixed layers (Table 2). No systematic variation with respect to the sample location is observed.

The analysed illite fractions are composed mainly of the $1M_d$ and $2M_1$ polytypes and only subordinate 1 M illite. The $1M_d$ polytype is dominant in the <0.2 μm fractions throughout all analysed samples. In the <2 μm fraction, the $1M_d$ is also the dominant polytype, except samples APG 91-09 and APG 92-09 showing the $2M_1$ polytype as dominant. The 2–6 μm fractions are mostly made up by $2M_1$ illite. The content of different polytypes correlates with obtained IC values (Table 2).

Zircon (U-Th)/He ages

The zircon samples yield (U-Th)/He ages between 276.8 ± 6.4 Ma (Early Triassic) and 141.5 ± 3.4 Ma (Early Cretaceous) showing a positive correlation with elevation (Fig. 9). The weighted means of the four samples vary from 263.6 Ma to 198.9 Ma (Table 3).

Apatite fission track ages

The three analysed samples show apparent apatite fission track ages that range between the Early Jurassic and the Early Cretaceous (Table 4). Although less constrained than in the (U-Th)/He ages, which is due to less analysed samples, a distinct positive correlation of age with increasing altitude is obvious between the samples APM 14-08 and APM 09-08 along the investigated elevation profile (Fig. 9). The apparent age of the topographic lower sample APM 14-08 is 143.7 ± 13.6 Ma, whereas APM 09-08 (on the top of the range) shows an age of 169.7 ± 14.4 Ma. However, an exception of this trend depicts APM 15-08. This sample is located at 831 m a.s.l. and has an apparent age of 196.1 ± 17.8 Ma (Table 4).

Regarding the fission track length, all three samples are characterised by distinct shortened tracks. The mean track length varies between 12.13 and 12.5 μm with s.d. of ±1.34–1.75 μm (Table 4). Further, the track length distribution of APM 15-08 and APM 14-08 is unimodal distributed (Fig. 9). In contrast, APM 09-08 is characterised by a bimodal track length distribution (Fig. 9). The mean Dpar values (etch pit diameter) for the three samples range between 1.64 and 1.75 μm (Table 4).
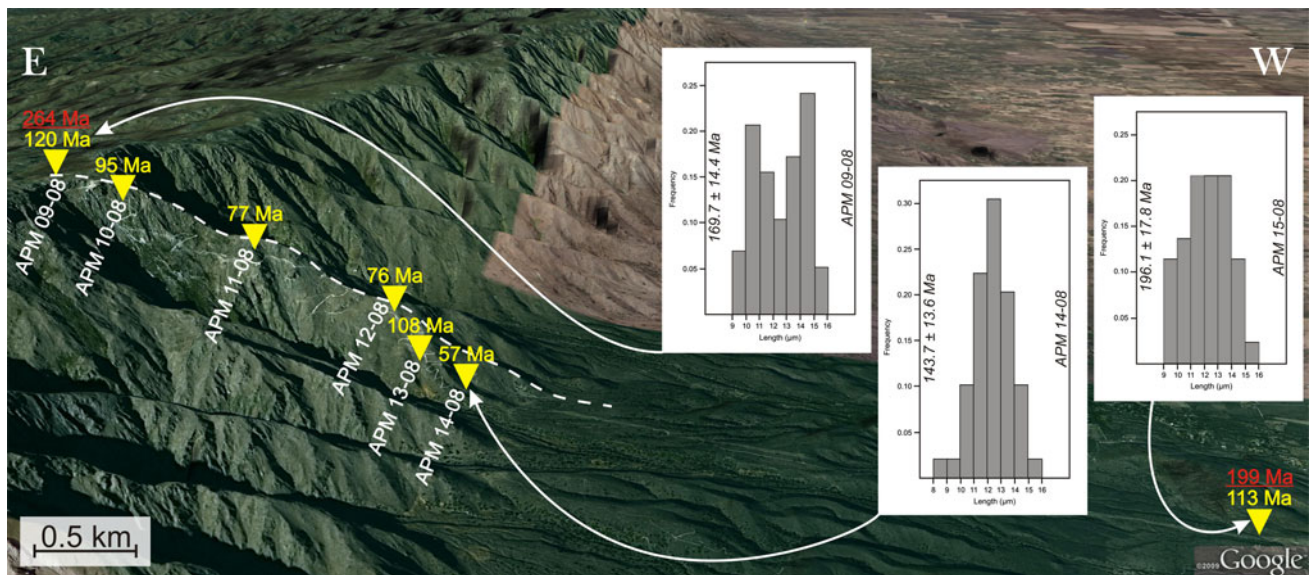
Fig. 9 Sampled elevation profile near Yacanto based on a satellite image from Google Earth pro[TM] (2010), which is vertically exaggerated by a factor of 1.25. The *yellow triangles* mark the sample locations and the *sample number* is indicated by the white font. Also inserted are the apatite (U-Th)/He ages (*yellow font*), the zircon (U-Th)/He ages (*red* and *underline font*), and the apparent apatite fission track ages with their associated track length distribution is shown by the diagrams (also contain the sample number). The *white, dashed line* indicates the morphology along the profile

Apatite (U-Th)/He ages

Apatite (U-Th)/He weighted mean ages vary from 57 Ma (APM 14-08) at the foothill to 108 Ma (APM 09-08) on the top of the profile showing a distinct positive correlation of age with increasing altitude (Fig. 9 and Table 3). The obtained ages of APM 11-08 and APM 12-08 are similar lying at around 75 Ma. In contrast, sample APM 10-08 is significantly older than APM 11-08.

Exceptions of the positive age with elevation correlation are represented by APM 13-08 and APM 15-08 (Fig. 9). These two samples show ages of 108.3 Ma and 113.3 Ma, respectively. The (U-Th)/He ages of every apatite sample are younger or overlap within their 1σ error with its corresponding AFT-age in this profile (Table 3 and 4).

Ar–Ar dating

Three trachyandesitic rock samples from discrete outcrops have been investigated (Fig. 1).

The sample APM 6-09 was taken from trachyandesitic lava in a near top position (approx. 1,950 m altitude) on the eastern side of Cerro Tomolasta. The rock displays a porphyritic texture and is build up by plagioclase, sanidine and amphibole phenocrysts in a fine-grained, dark grey groundmass of plagioclase, K-feldspar and amphibole. With 20–30 vol.% and up to 3 cm size, subhedral sanidine phenocrysts are the volumetrically dominant phase. The sample APM 7-09 represents a volcanic bomb, taken from a small outcrop within volcaniclastic layers on the southeastern slope of El Morro. The sample CT3 (Table 5) represents a trachyandesitic lava, taken from the slope of Cerro Tala, directly east of the Sierra de Morro, approx. 2.5 km south of the village La Esquina. This sample shows sanidine phenocrysts up to 5 mm (10–20 vol.%) as well as microcrysts of plagioclase, hornblende and pyroxene in a pale grey groundmass of feldspar, amphibole and pyroxene.

All samples show whole rock and hornblende spectra with well-defined flat plateaus (Fig. 10). The whole rock ages exhibit better constrained plateau ages due to smaller errors of their individual degassing steps (Table 5, shown in bold, Fig. 10). The obtained ages range from 7.54 ± 0.04 Ma for the Cerro Tomolasta (APM 6-09 WR) to 1.91 ± 0.02 Ma for the Cerro Tala (CT3 Hbl., Fig. 4).

Discussion

Constraints on regional cooling and fault activity by K–Ar dating

The high-temperature (>300°C) cooling history of the basement rocks of the Sierra de Comechingones was determined by K–Ar ages taken from biotite, muscovite and hornblende mineral separates from the hanging wall and footwall blocks of Guacha Corral shear zone, as well as from the shear zone itself (Steenken et al. 2010). The

Table 3 Zircon and apatite (U–Th)/He data of the samples from the elevation profile near Yacanto

Sample no. (rocktype)		^{4}He vol. [ncc]	SE [%]	^{238}U mass [ng]	SE [%]	^{232}Th mass [ng]	SE [%]	Th/U ratio	Sm mass [ng]	SE [%]	Ejection correct. (Ft)	Uncorrect. He age [Ma]	Ft-correct. He age [Ma]	1 s [Ma]	Sample weighted average age [Ma]
Zircon															
APM-09-08 (migmatite)	z1	85.368	1.6	3.186	1.8	0.533	2.4	0.2	0.070	7.5	0.80	209.6	262.6	6.2	
	z2	64.745	1.6	2.601	1.8	0.206	2.4	0.1	0.030	7.1	0.79	198.9	250.2	5.9	
	z3	135.567	1.6	4.397	1.8	1.262	2.4	0.3	0.077	10.1	0.85	234.3	276.8	6.4	263.6
APM-11-08 (granite)	z1	44.875	1.6	2.118	1.8	0.396	2.4	0.2	0.056	5.8	0.74	165.7	224.9	5.3	
	z2	35.791	1.6	1.494	1.8	0.133	2.5	0.1	0.010	6.3	0.75	191.1	255.7	6.1	
	z3	42.684	1.6	1.581	1.8	0.350	2.4	0.2	0.019	5.9	0.76	208.7	275.2	6.4	253.6
APM-12-08 (migmatite)	z1	23.449	1.6	1.056	1.8	0.081	2.5	0.1	0.004	6.9	0.73	177.9	242.9	5.8	
	z2	12.829	1.6	0.606	1.8	0.085	2.5	0.1	0.005	6.8	0.73	167.2	228.4	5.4	
	z3	12.208	1.6	0.584	1.8	0.093	2.5	0.2	0.006	6.7	0.74	164.5	223.8	5.3	232.0
APM-15-08 (granite)	z1	171.524	1.6	12.877	1.8	0.649	2.4	0.1	0.140	30.3	0.76	108.0	141.5	3.4	
	z2	81.171	1.6	4.470	1.8	1.480	2.4	0.3	0.890	29.6	0.76	137.7	181.2	4.2	
	z3	136.096	1.6	5.345	1.8	0.917	2.4	0.2	0.909	27.7	0.81	199.1	245.2	5.8	198.9
Apatite															
APM 9-08 (migmatite)	a1	1.876	1.7	0.119	1.9	0.006	5.7	0.05	0.880	5.1	0.83	120.1	145.2	3.5	
	a2	3.060	1.7	0.242	1.8	0.009	4.6	0.04	1.787	4.9	0.91	97.1	106.8	2.5	
	a3	0.507	1.9	0.051	2.2	0.001	17.6	0.02	0.397	4.9	0.83	76.7	92.6	2.5	
	a4	1.625	1.7	0.118	1.9	0.002	12.3	0.02	0.726	4.9	0.86	107.0	124.3	3.1	120.0
APM 10-08 (migmatite)	a1	0.859	1.8	0.073	2.0	0.004	7.2	0.05	1.074	5.8	0.85	85.8	100.9	2.5	
	a2	0.925	1.8	0.090	1.9	0.004	7.1	0.04	0.886	5.7	0.89	77.8	87.9	2.2	94.9
APM 11-08 (granite)	a1	0.115	2.3	0.017	4.6	0.000	638.9	0.00	0.223	5.0	0.75	50.3	67.0	3.1	
	a2	0.119	2.5	0.014	5.0	0.004	7.1	0.31	0.119	5.0	0.74	62.5	84.4	4.1	76.9
APM 12-08 (migmatite)	a1	0.133	2.4	0.021	3.0	0.009	4.50	0.41	0.607	5.7	0.86	39.0	45.2	1.5	
	a2	0.885	1.8	0.083	1.9	0.004	4.2	0.05	1.969	15.1	0.79	80.1	101.6	2.7	
	a3	1.085	1.7	0.151	1.8	0.004	4.3	0.03	1.160	15.7	0.80	53.3	66.7	1.9	
	a4	0.731	1.8	0.091	1.9	0.005	3.9	.06	1.209	16.0	0.75	59.4	79.0	2.3	77.5
APM 13-08 (migmatite)	a1	1.595	1.7	0.105	1.9	0.001	20.2	0.01	0.952	4.9	0.87	115.4	133.2	3.3	
	a2	0.970	1.8	0.114	1.9	0.003	4.7	0.03	1.209	16.4	0.71	63.8	89.7	2.5	
	a3	4.434	1.7	0.428	1.8	0.003	5.1	0.01	1.950	16.8	0.72	82.0	113.9	2.8	
	a4	1.259	1.7	0.143	1.8	0.003	5.3	0.02	2.046	17.1	0.73	64.8	88.8	2.6	108.3
APM 14-08 (migmatite)	a1	0.295	2.0	0.054	2.2	0.009	4.5	0.17	0.558	5.0	0.76	39.9	52.3	1.4	
	a2	0.396	1.9	0.059	2.1	0.003	8.2	0.06	0.352	4.8	0.76	52.2	68.5	1.9	
	a3	0.463	1.9	0.070	2.0	0.006	5.6	0.09	0.479	4.9	0.75	50.4	67.1	1.8	
	a4	0.055	3.1	0.014	4.7	0.001	32.4	0.05	0.0134	5.0	0.73	29.6	40.8	2.1	108.3
APM 15-08 (granite)	a1	1.742	1.7	0.102	1.9	0.069	2.7	0.67	2.044	4.9	0.81	106.2	130.5	3.0	56.7
	a2	1.820	1.7	0.118	1.9	0.245	2.5	2.08	2.476	5.0	0.89	76.4	85.9	1.9	113.3

^{4}He amount of in nano-cubic centimetre at standard pressure and temperature, *SE* standard error in percent, U^{238}/Th^{232} amount of in nanogram, *uncorrect. age* uncorrected age, *Ft* ejection correction factor calculated after Farley et al. (1996), *correct. age* corrected age, *1s* standard deviation

Table 4 Apatite fission track data of the samples from the elevation profile near Yacanto

Sample no. (rocktype)	Latitude longitude	Elevation (m)	n	ρ_s	N_s	ρ_i	N_i	ρ_d	N_d	$P(X^2)$ (%)	Age (Ma)	$\pm 1\sigma$ (Ma)	MTL (μm)	SD (μm)	N(L)	Dpar (μm)
APM 09-08 (migmatite)	32°03.252′ 064°56.157′	2682	25	20.83	2670	14.994	1922	7.66	7368	42	169.7	14.4	12.5	1.75	58	1.72
APM 14-08 (migmatite)	32°03.007′ 064°58.122′	1447	25	16.84	1279	14.404	1094	7.6	7368	2	143.7	13.6	12.3	1.34	50	1.75
APM 15-08 (granite)	32°02.818′ 065°01.761′	831	25	17.22	1612	11.016	1031	7.83	7368	10	196.1	17.8	12.13	1.67	61	1.64

n number of dated apatite crystals, ρ_s/ρ_i spontaneous/induced track densities ($\times 10^5$ tracks cm^{-2}), N_s/N_i number of counted spontaneous/induced tracks, N_d number of tracks counted on dosimeter, $P(X^2)$ probability obtaining chi-squared value (X^2) for n degree of freedom (where n is the number of crystals—1); age $\pm 1\sigma$ is central age ± 1 standard error (Galbraith and Laslett 1993); ages were calculated using zeta calibration method (Hurford and Green 1983); glass dosimeter CN-5, and zeta value of 323.16 ± 25.31 a cm^{-2}; *MTL* mean track length, *SD* standard deviation of track length distribution, *N* number of tracks measured, *Dpar* etch pit diameter

post-Pampean cooling of the basement of the Sierra de Comechingones took place in the Cambrian to Early Ordovician, as recorded by the K–Ar ages of pegmatitic hornblendes and muscovite booklets (513 Ma and 498 to 474 Ma, respectively). Based on the closure temperature for the K–Ar system between 500 and 430°C (for non-recrystallised, coarse-grained muscovite booklets; e.g. Kirschner et al. 1996; Villa 1998), these ages allow the estimation of a cooling rate of approximately 9°C/Ma after the Pampean granulite facies metamorphism (780–725°C, 6–5.5 kbar; Guereschi and Martino 2008). With a hypothetical geothermal gradient of 35°C/km, a maximum exhumation rate of about 0.1 mm/a can be estimated (Steenken et al. 2010). Middle to Late Silurian K–Ar biotite ages (426–420 Ma) document the cooling of the Sierra de Comechingones basement to approximately 300°C (e.g. Purdy and Jäger 1976) and the final transition from ductile to brittle deformation regime—between 290 and 300°C due to the onset of brittle behaviour of quartz below this temperature (e.g. van Daalen et al. 1999; Passchier and Trouw 2005 and references therein).

K–Ar data may also provide valuable information on fault activities by dating authigenic illites taken from fault gouges. In any case, the correlation of geological events and K–Ar ages from authigenic illite separates requires a careful consideration of the fundamental assumptions of the K–Ar-illite method (e.g. Clauer and Chaudhuri 1998).

One of the most important assumptions involved in the interpretation of K–Ar dating is a closed system behaviour, thus no gain or loss of either ^{40}K or ^{40}Ar after the formation of the illite. A lost of Ar might be possible due to thermal diffusion effects or exchange reactions with hydrothermal fluids (e.g. Villa 1998). The importance of the effective diffusion radius on the closure temperature for the Ar system has been demonstrated throughout a large number of publications (e.g. Dahl 1996; Villa 1998; Hodges 2003).

These publications are focused on white micas with grain sizes >200 μm. In case of illite fine fractions, available information is sparse. Hunziker et al. (1986) reported a closure temperature interval for the mica fractions <2 μm of 260 ± 30°C, whereas Wemmer and Ahrendt (1997) found indication that fine-grained white micas (sericite <2 μm) did not behave as open systems, even at temperatures of 275°C. Therefore, the closure temperature of fine-grained mica has to be estimated somewhere between 275 and 350°C (Wemmer and Ahrendt 1997). Furthermore, errors in the acquisition of accurate K–Ar ages can arise from contamination by other K-bearing phases. Potassium-feldspar for example can, even being very much older, rejuvenate the age due to its low closure temperature of about 150°C (e.g. Fitz-Gerald and Harrison 1993). The major problem, which must be considered, is the possible mixture of illite formed by different events at different times. For authigenic, neocrystallised illite, the finest illite fraction should represent the most recently grown illite. Coarser grain-size fraction should yield older ages representing earlier illite forming events (e.g. Clauer et al. 1997).

In this study, we used the different illite polytypes to decipher different illite forming events, thus the time span of the deformation history. In low-grade sedimentary rocks, the 2M$_1$ illite polytype is considered as detrital component, due to its restriction to epizonal conditions. The 1 M$_d$ and 1M polytypes are considered as authigenic products formed under diagenetic to anchimetamorphic, prograde conditions during subsequent burial (e.g. Grathoff and Moore 1996). In contrast to sedimentary environment, the illite investigated in this study originates from fault gouges developed from granitoid host rocks under retrograde conditions. Thus, the development of 2M$_1$ illite polytypes in a brittle fault gouge is possible due to subsequent cooling of the host rock and its passage through epizonal conditions, which are more or less equivalent with the ductile–brittle

Table 5 Results of Ar–Ar analyses on trachyandesites sampled within the La Carolina volcanic field and the Sierra del Morro

Sample no. (rocktype)	Locality latitude longitude	Mineral	Integrated age (Ma)	Plateau age (Ma)	Plateau information	Isochron age (Ma)	Isochron information
APM 6-09 (trachyandesite)	Cerro Tomolasta, La Carolina district $-32.812719°$ $-66.075278°$	WR	7.60 ± 0.04	**7.54 ± 0.04**	4 of 7 fractions, 89% ^{39}Ar release, MSWD $= 0.70$	7.45 ± 0.06	7 of 7 fractions, 89% $^{40}Ar/^{39}Ar_i = 312 \pm 5$, MSWD $= 1.86$
APM 7-09 (trachyandesitic lava bomb)	Cerro El Morro, El Morro district $-33.194399°$	WR	1.92 ± 0.02	**1.92 ± 0.03**	6 of 7 fractions, 99% ^{39}Ar release, MSWD $= 2.03$	1.95 ± 0.03	6 of 9 fractions, 89% $^{40}Ar/^{39}Ar_i = 293 \pm 2$, MSWD $= 1.71$
	$-65.377763°$	Hbl.	2.19 ± 0.15	2.17 ± 0.14	7 of 9 fractions, 98% ^{39}Ar release, MSWD $= 0.82$	2.10 ± 0.23	9 of 9 fractions, 89% $^{40}Ar/^{39}Ar_i = 296 \pm 2$, MSWD $= 0.96$
CT3 (trachyandesite)	Cerro Tala, El Morro district $\sim -33.165472°$	WR	1.87 ± 0.03	**1.91 ± 0.02**	4 of 7 fractions, 82% ^{39}Ar release, MSWD $= 0.00$	1.92 ± 0.03	6 of 7 fractions, 89% $^{40}Ar/^{39}Ar_i = 295 \pm 2$, MSWD $= 0.05$
	$\sim -65.366944°$	Hbl.	1.93 ± 0.12	1.90 ± 0.13	6 of 9 fractions, 87% ^{39}Ar release, MSWD $= 0.80$	1.85 ± 0.20	5 of 9 fractions, 89% $^{40}Ar/^{39}Ar_i = 296 \pm 3$, MSWD $= 1.29$
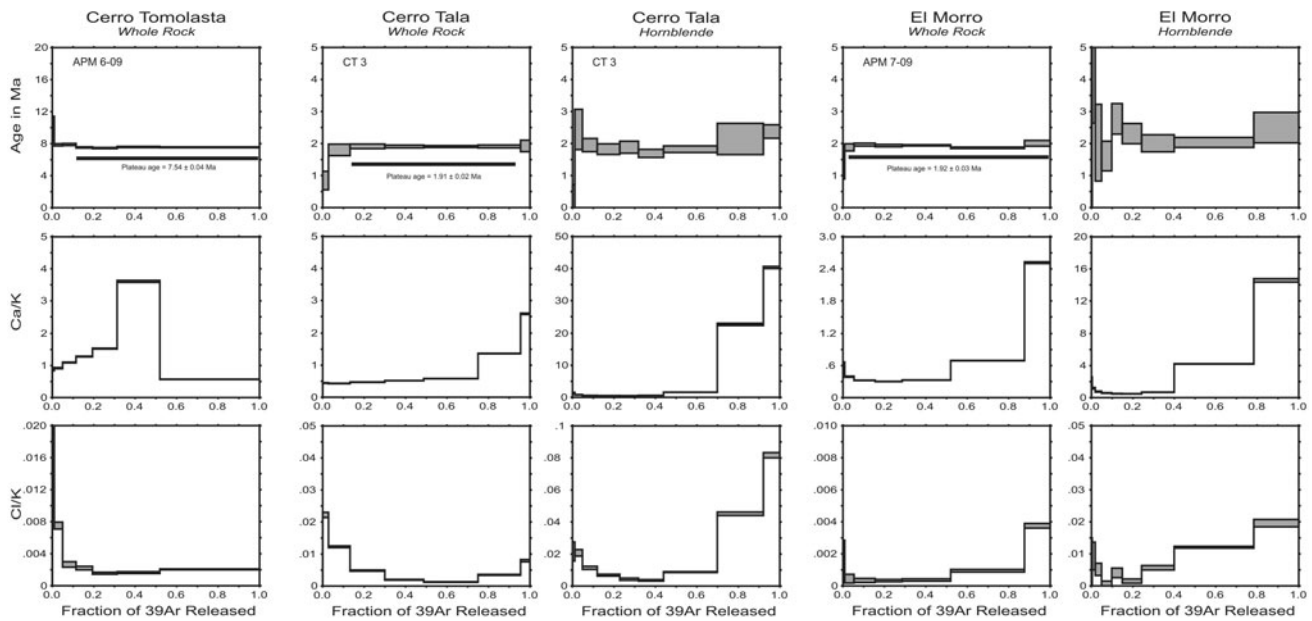
Fig. 10 Ar–Ar age spectra from analysed trachyandesites showing whole rock (WR) and hornblende ages. A sample is considered to have a plateau if it has 3 or more contiguous fractions constituting at least 50% ^{39}Ar release and is significant at the 95% confidence level (as indicated by an Mean Square Weighted Deviates; MSWD < ~2.5). A sample is considered to form an isochron if it has 3 or more contiguous fractions that form a linear array that is significant at the 95% confidence level (MSWD < ~2.5)

transition. Therefore, the 2M$_1$ polytype should record the onset of brittle deformation.

Contamination of mineral fine fractions (<2 μm, <0.2 μm) by cataclastically crushed muscovite of the host rock is very unlikely because of the very strong mechanical resistance of this mineral. Muscovite flakes would rather rotate parallel to the faulting plane than being grinded to extremely small particles (e.g. Wemmer 1991). If so, they could be identified by their excellent crystallinity (ca. 0.060 Δ°2θ).

Following the above stated assumptions, we interpret all illite to be neoformed, i.e. to be fault gouge related. Thus, the wide age span of the dated sample fractions documents a long lasting fault activity from 341 Ma to 174 Ma, whereby the relationship of increasing K–Ar ages with increasing grain size (Table 1; Fig. 8) is consistent with increasing content of older 2M$_1$ illite. Still, larger grain-size fractions have to be considered as mixtures of illites formed at different times and thus to be younger than the oldest illite forming event.

This interpretation is constrained by K–Ar ages from pegmatitic large-grained host-rock muscovites in the Merlo profile showing ages from 487 Ma to 431 Ma (Steenken et al. in review), thus they are significantly older than all obtained K–Ar illite ages, even from fractions with high 2M$_1$ polytype content (Table 1).

The six analysed fault gouge samples show three different age groups, depending on their location along the sampled profile (Fig. 8). The samples from the footslope of the Sierra de Comechingones (samples 91-09 and 92-09) show the oldest ages of all analysed samples. Neglecting a possible potassium contamination of the 2–6 μm fractions (Table 2), these samples are interpreted to document the onset of brittle deformation in this region. The onset of deformation under epizonal conditions is supported by the highest amount of 2M$_1$ illite polytype in all analysed samples (see Table 1). Thus, the oldest age of the 2–6 μm fraction of around 340 Ma (Fig. 8, APG 92-09) has to be considered as minimum age for the onset of brittle deformation in this region. This result is similar to a K–Ar muscovite age of 335 Ma from a fault scarp in the Sierras de Córdoba (Los Gigantes) obtained by Jordan et al. (1989). Additionally, this interpretation is supported by the mentioned K–Ar biotite ages from the Sierra de Comechingones, documenting the cooling below the ductile–brittle transition at Middle to Late Silurian times (K–Ar biotite ages, 426–420 Ma, Steenken et al. 2010). Deformation along the sampled faults in the footslope area ceased around 240 Ma, but brittle deformation continued along other faults, e.g. APG 82-09 to APG 90-09 (Fig. 8).

The samples taken from the uppermost hillslope area (APG 82-09 and 85-09) show a narrower age span between fractions than the other samples, indicating a shorter period of activity along these faults. We interpret the comparatively small age span of sample APG 82-09 to represent a major short-lived deformation event between 260 and 240 Ma without any further reactivation of this fault. The samples APG 89-09 and 90-09 derived from the middle slope area show the youngest ages of all samples. Activity along these faults is interpreted to have started at similar times than the

deformation on the uppermost hillslope area (around 260 Ma). The <2 μm fractions yield ages of 223 and 210 Ma. As these fractions include the younger <0.2 μm fractions the onset of brittle deformation around 260 Ma is likely, matching the ages obtained from the 2–6 μm fraction. This gives evidence to a major Permo-Triassic (240–260 Ma) deformation event, which might be related to an earlier flat-slab subduction episode with subsequent compression at these latitudes during the Early-Middle Permian as proposed by Ramos and Folguera (2009). This event might also be related to the Permian deformed rocks of the Bajo de Velis (e.g. Costa et al. 1998; Azcuy et al. 1999).

The <0.2 μm fraction documents a further reactivation around 175 Ma in the Middle Jurassic. This reactivation could be related to rifting processes in the region of the Sierras Pampeanas generated during the earliest stage of opening of the Southern Atlantic Ocean. These rifting processes are also documented by basaltic rocks at the Sierra de Las Quijadas (westernmost San Luis province), with K–Ar ages ranging from 164 to 107 Ma (González 1971; González and Toselli 1973; Yrigoyen 1975), 10–20 Ma younger than the youngest K–Ar age of 174 Ma (APG 90-09, <0.2 μm fraction). The latter age is also interpreted to represent the last illite forming deformation event in this region, while brittle faulting may have continued below illite forming temperatures. These temperatures are estimated to be approximately 75–110°C (e.g. Hamilton et al. 1992). Cooling below the illite forming temperature is constrained by apatite fission track and apatite (U-Th)/He ages from the Yacanto profile (Table 3). In fact, the youngest illites must overlap with the apatite fission track ages (cooling below 130–60°C), whereas the apatite (U-Th)/He ages (60–40°C) always must be younger. This can be observed for all analysed samples. Non-deformational illite formation by fluid percolation cannot be excluded but is unlikely due to consistency of the data set.

Implications of low thermochronology and Ar–Ar dating

Thermal modelling

Based on the apatite fission track ages and the length distribution as well as on the (U-Th)/He ages of zircon and apatite, thermal modelling on two samples was performed following the approach of Ketcham (2005) using HeFTy, a computer program, which comprises tools to obtain more information from thermochronometric data through forward and inverse modelling.

These samples were chosen due to their position on the top (APM 9-08) and at the base (APM 15-08) of the vertical profile, containing the longest thermal memory of all samples and information of the youngest PRZ passage event, respectively. Two constraints were set to the thermal modelling: (1) the beginning of the time–temperature path was constrained by the zircon (U-Th)/He data and (2) the end of the time–temperature paths was set to 17°C, according to annual mean temperatures in the study area (Müller 1996).

Both modelled samples show slow cooling until 210 Ma (APM 15-08) and 180 Ma (APM 09-08) (Fig. 11). Cooling rates are between 4°C/Ma and 1.5°C/Ma during this time, followed by a time of more or less constant temperature conditions, lasting for about 80 Ma. This behaviour is also confirmed by the length distribution of the apatite fission tracks (Fig. 9), indicating a slow to moderate cooling through the PAZ. Final cooling below the effective (U-Th)/He closure temperature of apatite started around 90 Ma for APM 09-08 showing a cooling rate of 1.75°C/Ma reaching near surface conditions at around 80 Ma. Additionally, modelling revealed a possible burial event between 130 and 90 Ma, which might be related to the Early Cretaceous rifting event mentioned earlier. In contrast to sample APM 09-08, the onset of final cooling for APM 15-08 is far less
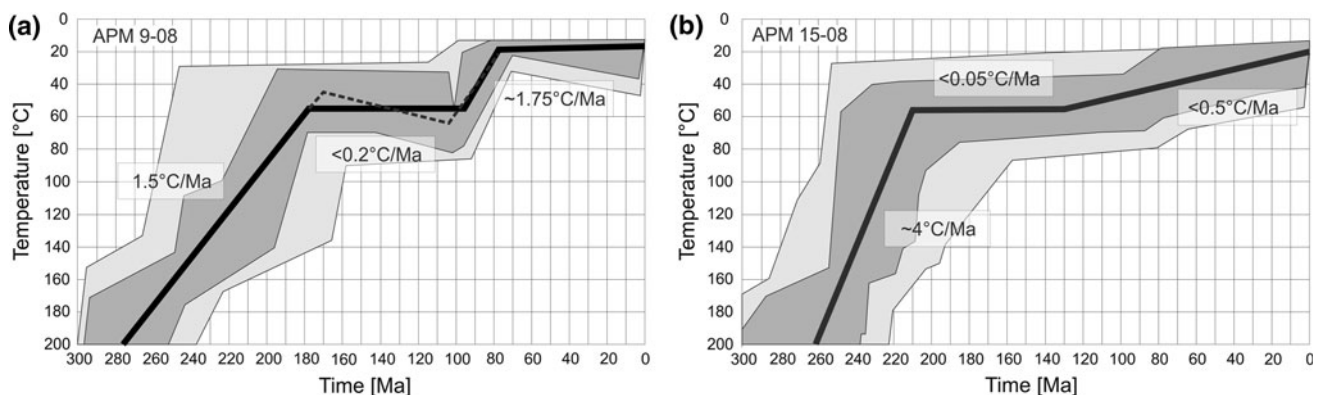
Fig. 11 Apatite fission track and (U-Th)/He thermal history modelling results using HeFTy (Ketcham 2005); light grey paths: acceptable fit, dark grey: good fit, black line: best fit. Also given are cooling rates considering the best fit path. **a** for sample APM 09-08. **b** for sample APM 15-08

Fig. 12 Elevation of the samples plotted against their AHe age showing a cluster at around 80 Ma indicating that they passed the PRZ at that time (e.g. Fitzgerald 2002; Fitzgerald et al. 1999, 2006). *Arrows* indicate shifting of the age after recalculating (further details are explained in the text). The grey area indicates an error in age of approximately 10 Ma. APM 13-08 is probably affected by a landslide
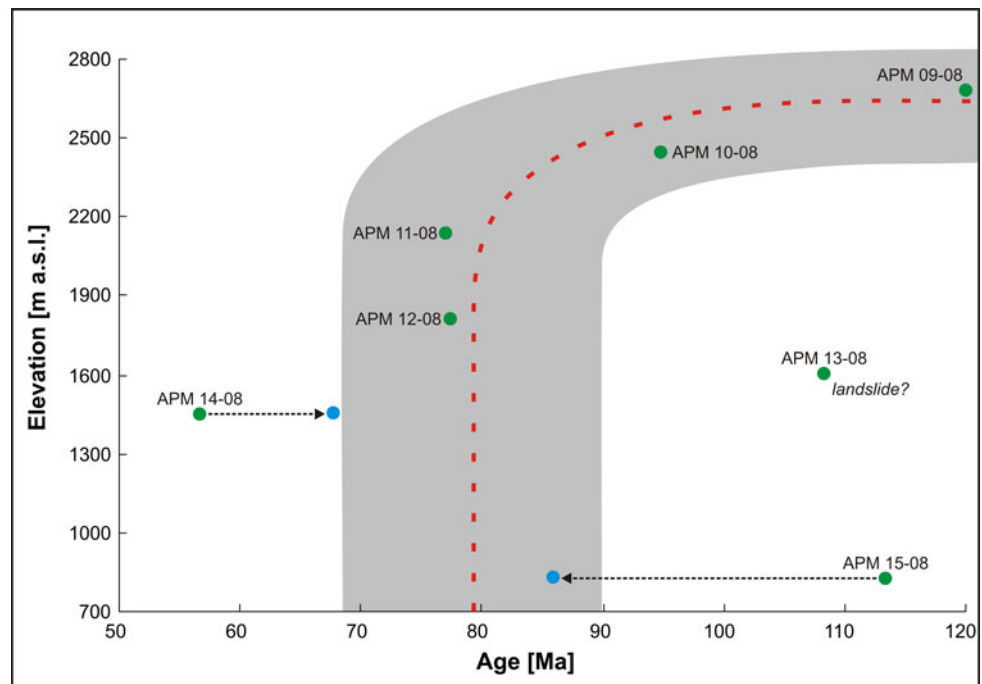
constrained. Cooling below 60°C probably started around 120 Ma with an average cooling rate of less than 0.5°C/Ma. However, these cooling rates are just a rough approximation concerning the possible range of good fitting time–temperature paths (Fig. 11), but are similar to cooling rates obtained by Jordan et al. (1989) based on fission track data from one single sample nearby the area regarded in this study.

A positive age-elevation trend, constrained by the used low-temperature geochronometers, usually allows a direct estimation of long-term exhumation rates, assuming that the closure isotherm of the employed systems remained flat and stationary during cooling (Stüwe et al. 1994). However, our samples are not from a pure vertical profile but show considerably horizontal distances between samples wherefore we abstained from calculating denudation rates.

AFT and AHe ages

Many apatite grains show (U-Th)/He ages around 70–80 Ma (Table 3) indicating cessation of the thermochronological record within the Yacanto profile implying that our samples left the PRZ at that time (Fig. 12; e.g. Fitzgerald 2002; Fitzgerald et al. 1999, 2006). Thus, no cooling history younger than Late Cretaceous is recorded by the used methods. The apparent Early Cretaceous ages of APM 13-08—APM 15-08 are too old and can be explained by (a) APM 13-08 is probably related to a rockslide evidenced in aerial photographs (b) a single grain age of APM 15-08 is contaminated by He-bearing inclusions. Excluding this single grain age, a weighted mean age

of 85 Ma is calculated still being older than sample APM 14-08. This discrepancy in the age-elevation trend is due to thrusting sample APM 14-08 above APM 15-08 (Fig. 13). This is also supported by the apatite fission track ages of these samples, indicating that APM 15-08 passed the partial annealing zone earlier than APM 14-08 (Fig. 9; Table 4). In contrast, the relatively decreased apatite (U-Th)/He age of APM 14-08 compared to the samples APM 11-08 and APM 12-08 is probably related to the small radius of crystal four which shows an age of around 40 Ma (Table 3). Rejecting this grain due to its size results in a mean age of nearly 70 Ma, confirming the mentioned time when the investigated samples left the PRZ (Fig. 12).

A geothermal gradient of approximately 26°C/km as suggested by Sobel and Strecker (2003) for the Northern Sierras Pampeanas was used to characterise the depth of the PRZ. Using this gradient, the upper thermal boundary of the PRZ is located in 2,300 m depth. Thus, the final exhumation, including the younger Andean deformation, is constrained to a maximum of 2,300 m since the passage of analysed samples through the PRZ at around 80–70 Ma. Due to the difference in elevation of approximately 1,850 m between sample APM 15-08 and APM 09-08 within the vertical profile, the amount of eroded thickness particularly at the hillslopes can be constrained to not exceed 450 m since 80 Ma. Otherwise, the apatite (U-Th)/He ages from the footslope area of the profile would yield younger ages. This information is used to calculate a very rough approximation of the erosion rate, affecting the top area of the profile, yielding a value of ≤6.4 m/Ma (0.006 mm/a). This does not contradict with the structural

Fig. 13 Uplift history of the Sierra de Comechingones implied by low-temperature geochronology. **a** Before 80 Ma, the area probably was characterised by a slightly elevated relief, hence acting as sedimentary source for adjacent basins to the east and northeast. Whether sedimentation also occurred to the west is arguable. Assuming a geothermal gradient of about 26°C/km, the PRZ of the (U-Th)/He system was located at 2300 m depth. All investigated samples lay within this PRZ before 80 Ma, whereby APM 15-08 was located at a higher crustal level than APM 14-08. **b** Currently, all investigated samples are at the surface and the PRZ is located at 2300 m depth assuming the same geothermal gradient. Due to passing the PRZ at around 80 Ma, indicated by the upper boundary of the paleo PRZ, the investigated samples could be uplifted by a maximum of 2300 m since the Late Cretaceous. The difference in altitude between APM 15-08 and APM 09-08 is 1850 m, representing the minimum amount of uplift. The maximum uplift of 2300 m is constrained by the depth of the paleo PRZ and a dip of 3° of the eastern slope. Also concerning erosional processes, the real uplift is in between these values since 80 Ma. Thrusting to the west along the main boundary fault located between APM 15-08 and APM 14-08 post 80 Ma resulted in the sample altitudes observed today
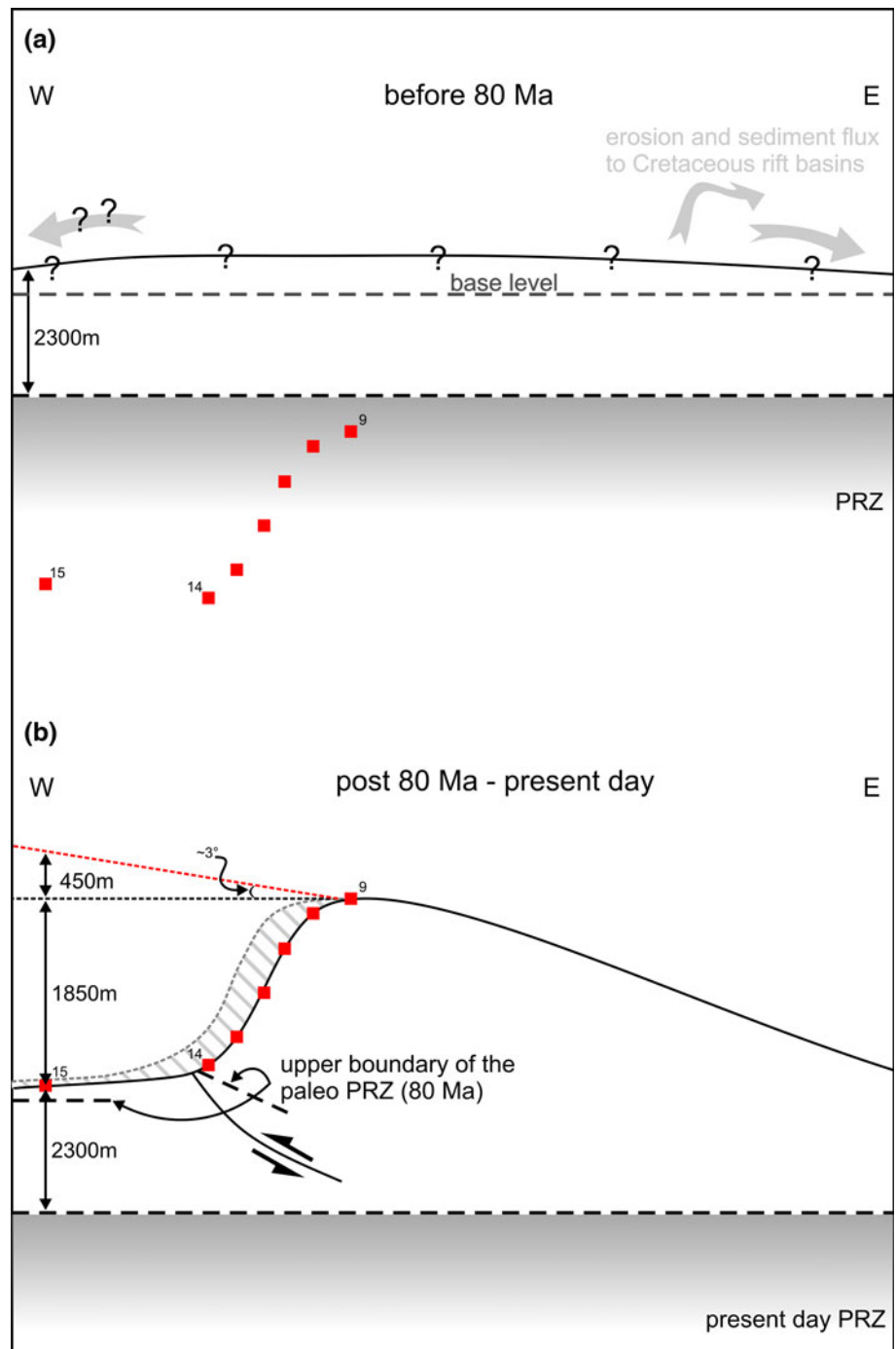
evolution model usually accepted for the Sierras Pampeanas (Criado Roque et al. 1981; Jordan and Allmendinger 1986; Costa 1992; Ramos et al. 2002; among others) but places rough constraints on the maximum possible uplift during the Andean orogeny (Fig. 13).

Low-temperature exhumation model

The exhumation history for the period before 80 Ma is less constrained due to the lack of zircon fission track data. Two scenarios can be discussed based on the obtained low-temperature data. First, the exhumation of our samples above the 60°C isotherm is induced by erosion commencing during the Early Cretaceous (Fig. 13). This suggests that the area of the Sierra de Comechingones was already characterised by a positive relief, a relatively stable setting, whereby the morphologic height acted as sedimentary source (Fig. 13a). The cooling path of APM 9-08 (Fig. 11a) shows a cooling rate of less than 0.2°C/Ma between 180 and 100 Ma, comparable to data described by

Jordan et al. (1989). Also, Carignano et al. (1999) postulated that the area of the Sierras Pampeanas was characterised by geomorphological positive elements showing evidence of erosional cycles forming several planation surfaces during the Jurassic and the Cretaceous. The related sediment flux was deposited in Cretaceous intracratonic rift basins (i.e. Sierra Chica Basin and General Levalle Basin) connected to the opening of the South Atlantic Ocean (Uliana et al. 1989; Schmidt et al. 1995; Webster et al. 2004). The sedimentary record represented by thick basal conglomerates in the General Levalle Basin or by two thick megasequences in the Sierra Chica Basin of up to 650 m. K–Ar ages of lava flows found in the basin deposits vary between 151 ± 10 Ma and 114 ± 5 Ma (Gordillo and Lencinas 1967; Stipanicic and Linares 1975).

The second scenario is characterised by a burial event between 130 and 90 Ma as indicated by thermal modelling and bimodal track length distribution of sample APM 09-08 (Figs. 11a and 9). The time–temperature path from thermal modelling indicates a maximum burial of approximately 2 km (Fig. 11a, dashed line). However, further data are needed to constrain this possible burial event.

Ar–Ar data on the age of volcanic activity

The Ar–Ar ages presented in this study strongly support and constrain the older K–Ar ages presented above (Table 5). Older K–Ar geochronological data as well as new Ar–Ar WR and mineral ages show that the volcanic rocks of the San Luis and Sierra de Morro area formed during a volcanic episode occurring between 11.2 and 1.9 Ma. The ages become progressively younger from the west to the east (Table 5). The volcanic activity of the belt began in the sectors of Cañada Honda and La Carolina between 11.2 and 8.2 Ma and expanded to the entire belt between 6.4 and 6.3 Ma (Ramos et al. 1991; Sruoga et al. 1996; Urbina and Sruoga 2008, 2009). The magmatic activity in the La Carolina region ceased around 6.3 Ma, whereas it lasted until 2.6 Ma in the Cerros del Rosario and the easternmost sector of El Morro and Cerro Tala. The westernmost sector of the Sierra del Morro shows activity until 1.9 Ma recording the youngest volcanic activity in the entire Sierras Pampeanas (Ramos et al. 1991; this study).

Conclusions

(1) K–Ar dating on illite fine fractions from fault gouges shows a long lasting brittle deformation history. The minimum age for the onset of brittle deformation is constrained to lay around 340 Ma. This is consistent with the 426–420 Ma K–Ar biotite ages from basement rocks (Steenken et al. 2010), which determine the brittle–ductile transition temperature.

(2) There is strong indication for a major Permo-Triassic (260–240 Ma) deformation event as indicated from several K–Ar illite fine fraction ages of all analysed fault gouge samples.

(3) The last illite forming event dated around 174 Ma, indicating cooling below the minimum formation temperature of illite.

(4) Assuming a geothermal gradient of 26°C/km, the thermochronological data constrain the total exhumation of the Sierra de Comechingones to a maximum of about 2.3 km since the passage of the analysed samples through the PRZ during the Late Cretaceous (80–70 Ma).

(5) Thermal modelling yields very low cooling rates, ranging from 4°C/km to <0.2°C/Ma.

(6) Regarding denudation processes, our thermochronological data indicate relatively stable conditions since at least 80 Ma. This fact agrees with the remarkable preservation of paleolandsurfaces at the eastern slope of the Comechingones uplifted block.

(7) The propagation of flat-slab subduction as expressed by volcanic activity is reconfirmed by new Ar–Ar data on amphiboles and whole rock, yielding ages from 7.54 to 1.92 Ma.

(8) Considering the present day difference in altitude between top and base of the Sierra de Comechingones (1,850 m), as well as the depth to the AHe paleo PRZ at 80 Ma, the amount of maximum eroded thickness from the top region of the Sierras can be constrained to a maximum of 450 m ever since, although more probably is close to zero.

(9) The new thermochronological data do not clearly illuminate the uplift of the Pampean ranges during the Neogene, but give indication that the Post-Cretaceous uplift related to the Comechingones fault at the study section is between 1850 m and 2300 m. However, several uncertainties related to the dynamic evolution of this structure might bias such estimation.

Appendix

Sample treatment and data acquisition (analytical techniques)

Each sampled fault gouge consists of approximately 250–1,000 g of fresh material. After careful selection, about 200 g of clay material was dispersed in distilled water and sieved <63 μm. The grain-size fractions <2 μm and 2–6 μm are gained from <63 μm fraction by differential settling in distilled water (Atterberg method following Stoke's law). Enrichment of the grain-size fraction <0.2 μm was accelerated by ultra-centrifugation. For details the reader is referred to Wemmer (1991). Following the concentration of the different grain-size fractions, the samples were subjected to isotope measurements for dating and X-ray diffraction for determining the mineralogy, IC and PT.

The XRD analysis was done using a Phillips PW 1800 X-ray diffractometer. For the identification of the mineral content a step scan (0.020°2θ) was performed in the range from 4 to 70°2θ. This was important to verify the existence of illite and to rule out the occurrence of any other potassium-bearing minerals. The mineral composition of all samples is shown in Table 2.

For the determination of the IC "thin" texture compounds according to Weber (1972) were prepared using 1.5 to 2.5 mg/cm^2 sample material. The metamorphic grade of the samples has been inferred from the peak width at half-height of the 10 Å peak (Kübler 1967) using a software algorithm developed at the University of Göttingen by Friedrich (1991), rewritten to FORTRAN by K. Ullmeyer (Geomar, Kiel) in 2005 (pers. com. K. Wemmer).

Digital measurement was carried out by a step scan with 301 points in a range of 7–10°2θ, using a scan step of 0.01°2θ and an integration time of 4 s per step and a receiving slit of 0.1 mm as well as an automatic divergence slit. The presence of mixed layer clays that may obliterate the 10 Å peak has been tested by duplicate determination of the material under air-dry and glycolated conditions. Results of the IC determination are shown in Table 3.

To determine the polytypism of illite, powder compounds were prepared and scanned in 561 steps in a range of 16–44°2θ, using a scan step of 0.05°2θ and an integration time of 30 s per step. The allocation of peaks to the corresponding polytypes was done as suggested by Grathoff and Moore (1996) and Grathoff et al. (1998). The randomness of orientation for the powder sample preparation was checked using the Dollase factor (Dollase 1986). We tried to quantify the amount of different polytypes by several methods as described by Reynolds (1963); Maxwell and Hower (1967); Caillère et al. (1982); Grathoff and Moore (1996) and Grathoff et al. (1998), but due to bad peak shapes none of the used methods yield reasonable data. For this reason the general abundance of the polytypes was estimated as suggested by Grathoff and Moore (1996). The abundance of different polytypes in the analysed samples is sown in Table 3.

Potassium and argon were determined following two different procedures. The argon isotopic composition was measured in a Pyrex glass extraction and purification vacuum line serviced with an on line ^{38}Ar spike pipette and coupled to a VG 1200 C noble gas mass spectrometer operating in static mode. Samples were pre-heated under vacuum at 120°C for 24 h to reduce the amount of atmospheric argon adsorbed onto the mineral surfaces during sample preparation. Argon was extracted from the mineral fractions by fusing samples using a low blank resistance furnace within the Pyrex glass extraction and purification line.

The amount of radiogenic ^{40}Ar was determined by isotope dilution method using a highly enriched ^{38}Ar spike (Schumacher 1975), which was calibrated against the biotite standard HD-B1 (Fuhrmann et al. 1987; Hess and Lippolt 1994). The released gases were subjected to a two-stage purification procedure via Ti-getters and SORB-ACs getters. Blanks for the extraction line and mass spectrometer were systematically determined and the mass discrimination factor was monitored by airshots. The overall error of the argon analysis is below 1.00%. Potassium was determined in duplicate by flame photometry using an Eppendorf Elex 63/61. The samples were dissolved in a mixture of HF and HNO$_3$. CsCl and LiCl were added as an ionisation buffer and internal standard, respectively. The pooled error of duplicate Potassium determination on samples and standards is better than 1%.

The K–Ar age were calculated based on the ^{40}K abundance and decay constants recommended by the IUGS quoted in Steiger and Jäger (1977). The analytical error for the K–Ar age calculations is given at a 95% confidence level (2σ). Analytical results are presented in Table 3. Details of argon and potassium analyses for the laboratory in Göttingen are given in Wemmer (1991).

AFT analytical techniques

Following standard density and magnetic mineral separation techniques, the apatite samples (Table 4) were mounted on a glass slide with epoxy. According to Donelick et al. (1999) the mounts were etched at 21°C for 20 s using 5.50 M nitric acid after grinding and polishing procedures in order to reveal spontaneous tracks within the apatite crystals. The external detector method described by Gleadow (1981) was used, whereby low-uranium muscovite sheets (Goodfellow mica) represent the external detector for induced tracks. For age determination, the zeta

calibration approach was adopted (Hurford and Green 1983) and 25 good-quality grains per sample were randomly selected and dated. The fission track ages were calculated using the software TRACKKEY version 4.2 (Dunkl 2002). Further, for all samples that had been dated ten Dpar measurements per grain were averaged to evaluate possible populations of different apatite compositions. Additionally, for track length analysis around 50–60 horizontal confined tracks of each sample were measured considering their angle to c-axis (Donelick et al. 1999).

(U-Th)/He analytical technique

For this work 2–4 apatite single crystals aliquots from seven samples (Table 3) as well as three zircon single crystals aliquots from four samples were carefully hand-picked using a binocular and petrologic microscopes. Only inclusion and fissure-free grains showing a well defined external morphology were used, whereas euhedral crystals were preferred. The shape parameters of each single crystal were determined, e.g. length and width, and archived by digital microphotographs in order to apply the correction of alpha ejection described by Farley et al. (1996). Subsequently, the crystals were wrapped in an approximately 1×1 mm sized platinum capsule and analysed following a two-stage analytical procedure (Reiners and Brandon 2006). This is characterised by (a) measuring the ^{4}He extraction, and (b) by analysing the ^{238}U, ^{232}Th and Sm content of the same crystal. During the first step, that was operated by HeLID automation software through a K8000/Poirot interface board, the Pt capsules were degassed in high vacuum by heating with an infrared diode laser. The extracted gas was purified using a SAES Ti-Zr getter at 450°C and the inert noble gases as well as a minor amount of rest gases were measured by a Hiden triple-filter quadrupole mass spectrometer equipped with a positive ion counting detector. Re-extraction was performed for each sample to control the quantitative amount of extracted helium. During the He measurement 240 readings of the mass spectrometer were recorded for every standard and sample.

After degassing, the samples were retrieved from the gas extraction line and spiked with calibrated ^{230}Th und ^{233}U solutions. Zircon crystals were dissolved in pressurised Teflon bombs using distilled 48% HF + 65% HNO$_3$ for five days at 220°C. For apatite 2% HNO$_3$ was used. These spiked solutions were then analysed by istope dilution method using a Perkin Elmer Elan DRC II ICP-MS provided with an APEX micro flow nebuliser.

To process and evaluate the He signal as well as the data of the ICP-MS measurements the factory-made software of the mass spectrometer MASsoft and the freeware software PEPITA, (Dunkl et al. 2008), were used. Regarding the latter evaluation, 40 to 70 readings of the ICP-MS were considered and individual outliers of the ^{233}U/^{238}U as well as ^{230}Th/^{233}Th ratios were tested and rejected according to the 2σ deviation criterion.

Finally, the raw (U-Th)/He ages of zircon and apatite were form-corrected (Ft correction) following Farley et al. (1996) and Hourigan et al. (2005). Replicate analyses of Durango apatite over the period of this study yielded a mean (U-Th)/He age of 30.4 ± 1.7 Ma, which is in good agreement with the reference (U-Th)/He age of 31.12 ± 1.01 Ma (McDowell et al. 2005). Replicate analyses of the Fish Canyon zircon standard yielded a mean (U-Th)/He age of 28.0 ± 1.6 Ma, which is also in good agreement with the reference Ar–Ar age of 27.9 ± 1.01 Ma (Hurford and Hammerschmidt 1985) and reference U/Pb-age of 28,479 ± 0.029 Ma (Schmitz and Bowring 2001).

Ar–Ar dating on trachyandesites

Samples were crushed, washed, sieved and hand-picked for small whole rock chips or minerals suitable for dating. The monitor mineral TCR-2 with an age of 27.87 Ma (Lamphere and Dylrymple 2000) was used to monitor neutron flux and calculate the irradiation parameter, J, for all samples. The samples and standards were wrapped in aluminium foil and loaded into aluminium cans of 2.5 cm diameter and 6 cm height. All samples were irradiated in position 5c of the uranium-enriched research reactor of McMaster University in Hamilton, Ontario, Canada for 0.75 megawatt-hours.

Upon their return from the reactor, the whole rock chips and grains of the monitor mineral were loaded into 2 mm diameter holes in a copper tray that was then loaded in an ultra-high vacuum extraction line. The monitors were fused, and samples heated, using an 8-watt argon-ion laser following the technique described in York et al. (1981), Layer et al. (1987) and Layer (2000). Multiple holes were heated at the same time to improve the signal. Argon purification was achieved using a liquid nitrogen cold trap and a SAES Zr-Al getter at 400°C for 20 min. The samples were analysed in a VG-3600 mass spectrometer controlled by either a Visual Basic operating program written in-house. The measured argon isotopes were corrected for system blank and mass discrimination, and for the irradiated samples, calcium, potassium and chlorine interference reactions, following procedures outlined in McDougall and Harrison (1999) and using the constants of Steiger and Jäger (1977). System blanks generally were 2×10^{-16} mol 40Ar and 2×10^{-18} mol 36Ar, which are 5 to 50 times smaller than fraction volumes. Mass discrimination was monitored by running both calibrated air shots and a zero-age glass sample. These measurements were made on a weekly to monthly basis to check for changes in mass

discrimination. Two runs of each sample were done, and the most precise run was chosen for presentation and discussion. Plateau and isochron analysis was done on all samples. A sample is considered to have a plateau if it has 3 or more contiguous fractions constituting at least 50% ^{39}Ar release and is significant at the 95% confidence level (as indicated by an Mean Square Weighted Deviates; MSWD < ~2.5). A sample is considered to form an isochron if it has 3 or more contiguous fractions that form a linear array that is significant at the 95% confidence level (MSWD < ~2.5). The choice of whether the plateau age or isochron age was determined by looking at the plots. If the isochron intercept was, within error, the same as the atmospheric value (^{40}Ar/^{36}Ar = 295.5) then generally the plateau age was chosen. A summary of the sample results is shown in Table 5.

References

Armstrong R (1966) K-Ar dating of plutonic and volcanic rocks in orogenic belts. Springer, Berlin, pp 117–133

Azcuy CL, Carrizo HA, Caminos R (1999) Carbonífero y Pérmico de las Sierras Pampeanas, Famatina, Precordillera, Cordillera Frontal y Bloque de San Rafael. Instituto de Geología y Recursos Minerales Geología Argentina 29:779–784

Bailey S (1966) The status of clay mineral structures. In: Proceedings of the 14th national conference on clays and clay minerals. Pergamon Press, New York, pp 1–23

Bailey S, Frank-Kamenetskii V, Goldstaub S, Kato A, Pabst A, Schulz H, Taylor H, Fleischer M, Wilson A (1977) Report of the international mineralogical association (IMA) international union of crystallography (IUCr) joint committee on nomenclature. Acta Crystallogr A 33(4):681–684

Baldwin S, Lister G (1998) Thermochronology of the South Cyclades Shear Zone, Ios, Greece: effects of ductile shear in the argon partial retention zone. J Geophys Res 103:7315–7336

Barazangi M, Isacks B (1976) Spatial distribution of earthquakes and subduction of the Nazca plate beneath South America. Geology 4:686–692

Cahill T, Isacks B (1992) Seismicity and the shape of the subducted Nazca plate. J Geophys Res 97:17503–17529

Caillère S, Henin S, Rautureau M (1982) Minéralogie des Argiles. Masson, Paris

Caminos R (1979) Sierras Pampeanas noroccidentales; Salta, Tucumán, Catamarca, La Rioja y San Juan. In: Turner JC (ed) Segundo Simposio de Geología Regional Argentina. Academia Nacional de Ciencias, Córdoba, pp 225–291

Carignano C, Cioccale M, Rabassa J (1999) Landscape antiquity of the central-eastern sierras pampeanas (Argentina): geomorphological evolution since gondwanic times. Zeitschrift für Geomorphologie 118:245–268

Clauer N, Chaudhuri S (1998) Isotopic dating of very low grade metasedimentary and metavolcanic rocks: techniques and methods. Blackwell, Cambridge, pp 202–226

Clauer N, Srodon J, Francu J, Sucha V (1997) K-Ar Dating of Illite—Fundamental Particles Separated from Illite-Smectite. Clay Miner 32(2):181–196. doi:10.1180/claymin.1997.032.2.02

Costa C (1987) Neotectónica de la sierra de San Luis: Resultados preliminares. In: X Congreso Geológico Argentino, Actas 1, Tucumán, pp 255–258

Costa C (1992) Neotectónica del sur de la Sierra de San Luis. Phd. Thesis [unpublished], Universidad Nacional de San Luis

Costa C (1996) Anállisis neotectónico en la sierra de San Luis y Comechingones: problemas y métodos. In: XIII Congreso Geológico Argentino, Actas 2, Buenos Aires, pp 285–300

Costa C (1999) Tectonica cuaternaria en las Sierras Pampeanas. Instituto de Geología y Recursos Minerales Geología Argentina 29:779–784

Costa C, Vita Finzi C (1996) Late Holocene faulting in the southeast Sierras Pampeanas of Argentina. Geology 24:1127–1130

Costa CH, Gardini CE, Schmidt CJ (1998) Dataciones 40Ar/39Ar y rasgos estructurales de la Formacion Cerro Varela (Triasico), Provincia de San Luis. Revista de la Asociacion Geologica Argentina 53(2):282–285

Costa C, Murillo V, Sagripanti G, Gardini C (2001) Quaternary intraplate deformation in the southeastern Sierras Pampeanas, Argentina. J Seismology 5:399–409

Costa C, Audermard F, Becerra F, Lavenu A, Machette M, París G (2006) An overview of the Main Quaternary Deformation of South America. Revista de la Asociación Geológica Argentina 61(4):461–479

Criado Roque P, Mombrú C, Moreno J (1981) Sedimentitas Mesozoicas. In: Yrigoyen M (ed) Geología y Recursos Naturales de la Provincia de San Luis, Relatorio 8° Congreso Geológico Argentino, pp 79–96

Dahl P (1996) The crystalchemical basis for Ar retention in micas: inferences from interlayer partitioning and implications for geochronology. Contrib Mineral Petrol 123:22–39

Dollase W (1986) Correction of intensities for preferred orientation in powder diffractometry: applications of the March model. J Appl Crystallogr 19:267–272

Donelick R, Ketcham R, Carlson W (1999) Variability of apatite fission-track annealing kinetics: II. Crystallographic orientation effects. Am Mineral 84:1224–1234

Dunkl I (2002) TRACKKEY: a Windows program for calculating and graphical presentation of fission-track data. Comput Geosci 28:3–12

Dunkl I, Mikes T, Simon K, von Eynatten H (2008) Brief introduction to the Windows program Pepita: data visualization, and reduction, outlier rejection, calculation of trace element ratios and concentrations from LAICPMS data, Mineralogical Association of Canada, Short Course 40, pp 334–340

Ehlers TA, Willett SD, Armstrong PA, Chapman DS (2003) Exhumation of the central Wasatch Mountains, Utah: 2. Thermokinemtaic model of exhumation, erosion, and thermochronometer interpretation. J Geophys Res 108:2173

England P, Molnar P (1990) Surface uplift, uplift of rocks, and exhumation of rocks. Geology 18:1173–1177

Farley KA (2002) (U-Th)/He dating: techniques, calibrations, and applications. In: Porcelli D, Ballentine CJ, Wieler R (eds) Noble gases in Geochemistry and Cosmochemistry, Reviews in Mineralogy and Petrology, Mineralogical Society of America, pp 819–844

Farley KA, Wolf R, Silver L (1996) The effects of long alpha stopping distances on (UTh)/He ages. Geochim Cosmochim Acta 60(21):4223–4229. doi:10.1016/S00167037(96)001937

Fitzgerald P (2002) Tectonics and landscape evolution of the Antarctic plate since the breakup of Gondwana, with an emphasis on the West Antarctic Rift System and the Transantarctic Mountains. R Soc New Zealand Bull 35:453–469

Fitz-Gerald J, Harrison T (1993) Argon diffusion domains in K-feldspar; I, Microstructures in MH10. Contrib Mineral Petrol 113:367–380

Fitzgerald P, Muñoz J, Coney P, Baldwin S (1999) Asymmetric exhumation across the Pyrenean orogen: implications for the tectonic evolution of a collisional orogen. Earth Planet Sci Lett 173:157–170

Fitzgerald P, Baldwin S, Webb L, O'Sullivan P (2006) Interpretation of (U–Th)/He single grain ages from slowly cooled crustal terranes: a case study from the Transantarctic Mountains of southern Victoria Land. Chem Geol 225:91–120

Friedrich D (1991) Eine neue Methode zur Bestimmung der Illit Kristallinität mit Hilfe digitaler Meßwerterfassung. Diploma thesis [unpublished], University of Göttingen

Fuhrmann U, Lippolt H, Hess J (1987) Examination of some proposed K-Ar standards: 40Ar/39Ar analyses and conventional K-Ar data. Chem Geol 66:41–51

Galbraith R, Laslett G (1993) Statistical models for mixed fission track ages. Nucl Tracks Radiat Meas 21:459–470

Gallagher K, Brown RW, Johnson C (1998) Fission track analysis and its application to geological problems. Earth Planet Sci Lett 26:519–572

Gleadow A (1981) Fission-track dating methods: what are the real alternatives. Nucl Tracks Radiat Meas 5:3–14

Gleadow A, Fitzgerald P (1987) Uplift history and structure of the Transantarctic Mountains: new evidence from fission-track dating of basement apatites in the Dry Valley area, southern Victoria Land. Earth Planet Sci Lett 82:1–14

González R (1971) Edades radimétricas de algunos cuerpos eruptivos de Argentina. Revista de la Asociación Geológica Argentina 26:411–412

González Bonorino F (1950) Lagunos problemas geológicas de las Sierras Pampeanas. Revista de la Asociación Geológica Argentina 5:81–110

González Díaz EF (1981) Geomorfología. In: Yrigoyen M (ed) Geología y Recursos Naturales de la Provincia de San Luis, Relatorio 8° Congreso Geológico Argentino, pp 193–236

González R, Toselli A (1973) Las rocas efusivas básicas de la Sierra de Las Quijadas al oeste de Hualtarán, Provincia de San Luis. Acta Geológica Lilloana 12:89–104

Gordillo C, Lencinas A (1967) Geología y petrología del extreme norte de la Sierra de Los Cóndores, Córdoba. Bol Acad Nac Cienc, Córdoba XLVI, pp 73–108

Gordillo C, Lencinas A (1979) Sierras Pampeanas de Córdoba y San Luis. In: Turner J (ed) Segundo Simposio de Geología Regional Argentina. Academia Nacional de Ciencias, Córdoba, pp 577–650

Grathoff G, Moore D (1996) Illite polytype quantification using Wildfire calculated Xray diffraction patterns. Clays Clay Miner 44(6):835–842

Grathoff G, Moore D, Hay R, Wemmer K (1998) Illite polytype quantification and K/Ar dating of paleozoic shales: a technique to quantify diagenetic and detrital illite. In: Schieber J, Zimmerle W, Sethi P (eds) Shales and Mudstones II. Schweizerbart, Stuttgart, pp 161–175

Guereschi AB, Martino RD (2008) Field and textural evidence of two migmatization events in the Sierras de Córdoba, Argentina. Gondwana Res 13(2):176–188

Guinier A, Bokij G, Boll-Dornberger K, Cowley J, Ďurovič S, Jagodzinski H, Krishna P, de Wolff P, Zvyagin B, Cox D, Goodman P, Hahn T, Kuchitsu K, Abrahams S (1984) Nomenclature of polytype structures—report of the international union of crystallography Ad-Hoc committee on the nomenclature of disordered, modulated and polytype structures. Acta Crystallogr A Found Crystallogr 40(4):399–404. doi:10.1107/S0108767384000842

Hamilton P, Giles M, Ainsworth P (1992) K–Ar dating of illites in Brent Group reservoirs: a regional perspective. Geological Society of London, Special Publication 61:377–400

Hess J, Lippolt H (1994) Compilation of K/Ar measurements on HDB1 standard biotite; 1994 status report. In: Odin G (ed) Phanerozoic Time Scale, Bulletin de Liaison et d'information. IUGS Subcommision on Geochronology, Paris, pp 19–23

Hodges K (2003) Geochronology and thermochronology in orogenic systems. Elsevier, Amsterdam, pp 263–292

Hourigan JK, Reiners PW, Brandon MT (2005) U/Th zonation dependent alpha ejection in (UTh)/He chronometry. Geochim Cosmochim Acta 96(13):3349–3365

Hunziker J, Fray M, Clauer N, Dallmeyer RD, Friedrichsen H, Flehming W (1986) The evolution of the illite to muscovite: mineralogical and isotope data from the Glarus Alps, Switzerland. Contr Mineral Petrol 92:157–180

Hurford A, Green P (1983) The zeta age calibration of fission-track dating. Chem Geol 41:285–317

Hurford A, Hammerschmidt K (1985) 40Ar-39Ar and K-Ar dating of the Bishop and Fish Canyon tuffs: calibration ages for fission track dating standard. Chem Geol (Isotope Geoscience Section) 58:23–32

Hurley P (1954) The helium age method and the distribution and migration of helium in rocks. Wiley, New York, pp 301–329

Introcaso A, Lion A, Ramos V (1987) La estructura profunda de las Sierras de Córdoba. Revista de la Asociación Geológica Argentina 42(5):117–178

Jordan T, Allmendinger R (1986) The Sierras Pampeanas of Argentina: a modern analogue of Rockey Mountain foreland deformation. Am J Sci 286:737–764

Jordan T, Zeitler P, Ramos V, Gleadow A (1989) Thermochronometric data on the development of the basement peneplain in the Sierras Pampeanas. J South Am Earth Sci 2(3):207–222

Jordan T, Isacks B, Allmendinger R, Brewer J, Ramos V, Ando C (1983) Andean tectonics related to geometry of subducted Nazca plate. Geol Soc Am Bull 94(3):341–361

Kay S, Gordillo C (1994) Pocho volcanic rocks and the melting of depleted continental lithosphere above a shallowly dipping subduction zone in the Central Andes. Contrib Mineral Petrol 117(1):25–44

Kay S, Mpodozis C, Ramos V, Munizaga F (1991) Magma source variations for mid-late Tertiary magmatic rocks associated with a shallowing subduction zone and thickening crust in the Central Andes (28–33°S), Geological Society of America Special Paper 26, pp 113–137

Kerrich R, Goldfarb R, Groves D, Garwin S (2000) The geodynamics of world-class gold deposits: characteristics, space-time distribution, and origins. In: Hagemann SG, Brown PE (eds) Gold in 2000. Society of Economic Geologists, Reviews in Economic Geology vol 13, pp 501–551

Ketcham R (2005) Forward and inverse modelling of low-temperature thermochronometry data. Rev Mineral Geochem 58:275–314

Ketcham R, Donelick R, Carlson W (1999) Variability of apatite fission-track annealing kinetics: III. Extrapolation to geological time scales. Am Mineral 84:1235–1255

Kirschner D, Hunziker J, Cosca M (1996) Closure Temperature of argon in micas; a review and reevaluation based on Alpine samples. Abstr Programs Geol Soc Am 28(7):441

Kralik M, Klima M, Riedmüller G (1987) Dating fault gouges. Nature 327:315–317

Kramer P, Escayolo M, Martino R (1995) Hipótesis sobre la evolución tectónica neoproterozoica de las Sierras Pampeanas de Córdoba (30°40′–32°40′), Argentina. Revista de la Asociación Geológica Argentina 50(14):47–59

Kübler B (1964) Les argiles indicateurs de métamorphisme. Revue de l'institute Francais du Petrolé 19:1093–1112

Kübler B (1967) La cristallinité de l'illite et les zones tout à fait supérieures du métamorphism. Etages Tectonique, Colloque de Neuchâtel, Neuchâtel

Kübler B (1968) Evaluation quantitative du métamorphisme par la cristallinité de l'illite. Bull Centre rech. Pau-SNPA 2:385–397

Lamphere M, Dylrymple G (2000) First-principles calibration of 38Ar tracers: Implications for the age of 40Ar/39Ar fluence monitors. US Geol Surv Prof Pap 1621:10

Layer P (2000) Argon40/argon39 age of the El'gygytgyn impact event, Chukotka, Russia. Meteoritics Planetary Sci 35:591–599

Layer P, Hall C, York D (1987) The derivation of 40Ar/39Ar age spectra of single grains of hornblende and biotite by laser step heating. Geophys Res Lett 14:757–760

Llambías E, Brogiono N (1981) Magmatismo Mesozoico y Cenozoico. In: Yrigoyen M (ed) Geología y Recursos Naturales de la Provincia de San Luis. VIII Congreso Geológico Argentino, San Luis, pp 101–115

Lyons JB, Snellenburg J (1971) Dating faults. Geol Soc Am Bull 82(6):1749–1752

Massabie A (1976) Estructura cenozoica entre Charbonier y Cosquín, Provincia de Córdoba. In: 6 Congreso Geológico Argentino, Actas 1, Buenos Aires, pp 109–123

Massabie A (1987) Neotectónica y sismicidad en la región de Sierras Pampeanas Orientales, Sierras de Córdoba, Argentina. In: 10 Congreso Geológico Argentino, Actas 1, pp 271–274

Maxwell D, Hower J (1967) Highgrade diagenesis and low-grade metamorphism of illite in the Precambrian Belt Series. Am Mineral 52:843–857

McDougall I, Harrison T (1999) Geochronology and Thermochronology by the 40Ar/39Ar method, 2nd edn. Oxford University Press, New York

McDowell F, McIntosh W, Farley K (2005) A precise Ar40Ar39 reference age for the Durango apatite (U-Th)/He and fission-track dating standard. Chem Geol 214:249–263

Miller H, Söllner F (2005) The Famatina complex (NW Argentina): back docking of an island arc or terrane accretion? Early Palaeozoic geodynamics at the western Gondwana margin, Geological Society of London, Special Publications 246, pp 241–256

Müller M (1996) Handbuch ausgewählter Klimastationen der Erde, 5th edn. Universität Trier FB VI, Trier

Pardo Casas F, Molnar P (1987) Relative motion of the Nazca (Farallón) and South American Plates since Late Cretaceous time. Tectonics 6(3):233–248

Passchier C, Trouw R (2005) Microtectonics, 2nd edn. Springer, Berlin

Pilger R (1981) Plate reconstruction, aseismic ridges, and low-angle subduction beneath the Andes. Geol Soc Am Bull 92:448–456

Purdy J, Jäger E (1976) K-Ar ages on rock-forming minerals from the Central Alps. Mem 1st Geol Min 30:31

Ramos V (1988) Late Proterozoic-Early Paleozoic of South America A collision history. Episodes 11:168–174

Ramos V (2009) The Grenville-Age basement of the andes. J South Am Earth Sci. doi:10.1016/j.jsames.2009.09.004

Ramos V, Folguera A (2009) Andean flat-slab subduction through time. Geol Soc London Spec Publication 327:31–54

Ramos V, Munizaga F, Kay S (1991) El magmatismo cenozoico a los 33°S de latitud: Geochronología y relaciones tectónicas. In: VI Congreso Geológico Chileno, Actas 1, pp 892–896

Ramos V, Escayola M, Mutti D, Vujovich G (2001) Proterozoic-Early Paleozoic ophiolites in the Andean basement of southern South America, Geological Society of America Special Paper 349, pp 331–349

Ramos V, Cristallini EO, Pérez DJ (2002) The Pampean flat-slab of the central Andes. J South Am Earth Sci 15:59–78

Regnier M, Chatelain JL, Smalley R, Ming Chiu J, Isacks BL, Puebla N (1992) Seismotectonic of the Sierra Pie de Palo, a basement block uplift in the Andean foreland, Argentina. Bull Seismological Soc Am 82:2549–2571

Reiners P, Brandon M (2006) Using Thermochronology to understand Orogenic Erosion. Annu Rev Earth Planet Sci 34:419–466

Reynolds R (1963) Potassium-Rubidium ratios and polytypism in illites and microclines from the clay size fractions of Proterozoic carbonate rocks. Geochim Cosmochim Acta 27:1097–1112

Reynolds R, Thomson C (1993) Illite from the Potsdam sandstone of New York: A probable noncentrosymetric mica structure. Clays Clay Miner 41:66–72

Rossello E, Mozetic M (1999) Caracterizacion estructural y significado geotectonico de los depocentros creacios continentales del centro-oesteargentine. 5 Simposio sobre o Cretaceo do Brasil. Boletim 5:107–113

Schmidt C, Astini R, Costa C, Gardini C, Kraemer P (1995) Cretaceous rifting, alluvial fan sedimentation, and Neogene inversion, southern Sierras Pampeanas, Argentina, AAPG Memoir 62, pp 341–358

Schmitz M, Bowring S (2001) U-Pb zircon and titanite systematics of the Fish Canyon Tuff: an assessment of high-precision U-Pb geochronology and its application to young volcanic rocks. Geochim Cosmochim Acta 65:2571–2587

Schumacher E (1975) Herstellung von 99, 9997% 38Ar für die 40 K/40Ar Geochronologie. Geochronologia Chimica 24:441–442

Smalley RJ, Isacks B (1987) A high resolution study of the Nazca plate Wadati-Benioff zone under western Argentina. J Geophys Res 92:13903–13912

Smalley RJ, Isacks B (1990) Seismotectonics of thin and thick-skinned deformation in the Andean foreland from local network data: evidence for a seismogenic lower crust. J Geophys Res 95:12487–12498

Sobel E, Strecker M (2003) Uplift, exhumation and precipitation: tectonic and climate control of late Cenozoic landscape evolution in the northern Sierras Pampeanas, Argentina. Basin Res 15:431–451

Środoń J, Eberl D (1984) Illite. Rev Mineral Geochem 13(1):495–544

Sruoga P, Urbina N, Malvicini L (1996) El Volcanismo Terciario y los Depositos Hidrotermales (Au, Cu) asociados en La Carolina y Diente Verde, San Luis, Argentina. In: XIII Congreso Geológico Argentino y III Congreso Exploracíon de Hidrocarburos, Actas 3, pp 89–100

Steenken A, López De Luchi M, Siegesmund S, Wemmer K, Pawlig S (2004) Crustal provenance and cooling of basement complexes of the Sierra de San Luis: An insight into the tectonic history of the proto-Andean margin of Gondwana. Gondwana Res 7(4):1171–1195

Steenken A, Wemmer K, Martino R, López De Luchi M, Gueresci A, Siegesmund S (2010) Post-Pampean cooling and the exhumation of the Sierras Pampeanas in the West of Córdoba (Central Argentina). Neues Jahrbuch für Geologie und Paläontologie Abhandlungen

Steiger R, Jäger E (1977) Subcommission on geochronology: convention on the use of decay constants in geo- and cosmochronology. Earth Planet Sci Lett 36:359–362

Stipanicic P, Linares E (1975) Catálogo de edades Radiométricas determinadas para la República Argentina. Asociatión Geológica Argentina, Publication Especial (Serie B) 3

Stockli DF, Farley KA, Dumitru TA (2000) Callibration of the apaptite (U-Th)/He thermochronometer on an exhumed fault block, White Mountains, California. Geology 28:983–986

Stüwe K, White L, Brown R (1994) The influence of eroding topography on steady-state isotherms: application to fission-track analysis. Earth Planet Sci Lett 124:63–74

Uliana MA, Biddle KT, Cerdan J (1989) Mesozoic extension and the formation of Argentine sedimentary basins. AAPG Memoir 46:599–614

Urbina N (2005) Cenozoic magmatism and mineralization in the Sierras Pampeanas of San Luis. In: Geological Society of Nevada Symposium 2005: Window to the World, Reno, pp 787–796

Urbina N, Sruoga P (2008) K-Ar mineral age constraints on the Diente Verde porphyry deposit formation, San Luis, Argentina. In: 6° South American Symposium on Isotope Geology (Bariloche), Extended Abstracts 37:4

Urbina N, Sruoga P (2009) La Faja Metalogenética de San Luis, Sierras Pampeanas: Mineralizacíon y Geochronología en el Contexto Metalogenético Regional. Revista de la Asociación Geológica Argentina 64(4):635–645

Urbina N, Sruoga P, Malvicini L (1997) Late Tertiary gold-bearing volcanic belt in the Sierras Pampeanas of San Luis, Argentina. Int Geol Rev 39:287–306

van Daalen M, Heilbronner R, Kunze K (1999) Orientation analysis of localized shear deformation in quartz fibres at the brittle-ductile transition. Tectonophysics 303:83–107

Villa I (1998) Isotopic closure. Terra Nova 10:45–47

Wagner G, Van Den Haute P (1992) Fission-track dating. Enke, Stuttgart

Weber K (1972) Notes on the determination of illite crystallinity. Neues Jahrbuch für Geologie und Paläontologie Monatshefte 6:267–276

Webster R, Chebli G, Fischer J (2004) General Levalle basin, Argentina: a frontier Lower Cretaceous rift basin. AAPG Bull 88(5):627–652. doi:10.1306/01070403014

Wemmer K (1991) K/Ar-Alterdatierungsmöglichkeiten für retrograde Deformationsprozesse im spröden und duktilen Bereich Beispiele aus der KTB Vorbohrung (Oberpfalz) und dem Bereich der Insubrischen Linie (N-Italien). Göttinger Arbeiten zur Geologie und Paläontologie 51:1–61

Wemmer K, Ahrendt H (1997) Comparative K-Ar and Rb-Sr age determinations of retrograde processes on rocks from the KTB deep drilling project. Geologische Rundschau 86:272–285

Wolf R, Farley K, Silver L (1996) Helium diffusion and low-temperature thermochronology of apatite. Geochim Cosmochim Acta 60:4231–4240

Wolf R, Farley K, Kass D (1998) Modeling of the temperature sensitivity of the apatite (U-Th)/He thermochronometer. Chem Geol 148:105–114

Yañez G, Ranero G, von Huene R, Díaz J (2001) Magnetic anomaly interpretation across a segment of the Southern Central Andes (32°–34°S): implications on the role of the Juan Fernández Ridge in the tectonic evolution of the margin during upper Tertiary. J Geophys Res 106:6325–6345

York D, Hall C, Yanase Y, Hanes J, Kenyon W (1981) 40Ar/39Ar dating of terrestrial minerals with a continuous laser. Geophys Res Lett 8:1136–1138

Yrigoyen MR (1975) La edad Creácica del Grupo del Gigante (San Luis) y su relacón con cuencas circunvecinas. Actas Primero Congreso Argentino de Paleontología y Bioestratigrafía 2:29–56

Zambrano G, Suvires J (2008) Actualización en el límite entre Sierras Pampeanas occidentales y Precordillera Oriental; en la provincia de San Juan. Revista de la Asociación Geológica Argentina 63(1):110–116

Zapata T, Allmendinger R (1996) La estructura cortical de la Precordillera Oriental y valle del Bermejo a los 30° de latitud sur. In: XIII Congreso Geológico Argentino, Actas 2, pp 211–224